

Initial results from marine sediment cores from the east-central Ross Sea

KATHY J. LICHT and DENIS DURAN, *Department of Geological Sciences and Institute for Arctic and Alpine Research, University of Colorado, Boulder, Colorado 80309*

We are currently analyzing marine sediment cores collected aboard the *Nathaniel B. Palmer* in the Ross Sea during the 1994 and 1995 field seasons. These cores were collected to help fulfill the goal of understanding the past behavior of the west antarctic ice sheet set forward by the West Antarctic Ice Sheet Initiative (Bindshadler 1995). Previous research on western Ross Sea cores (collected on *Eltanin* and *Deep Freeze* cruises) has been used to show that the ice did not advance to the continental shelf edge during marine isotope stage 2 (Licht 1995; Licht et al. in press) and provided carbon-14 (^{14}C) dates that constrain the timing of ice retreat across the continental shelf (Licht et al. 1996). In addition to these results, a bathymetric high has been recognized in the western Ross Sea based on seismic data and is interpreted as a grounding-line feature (Shipp and Anderson 1994); this feature probably represents the last-glacial-maximum grounding-line position.

Our objective is to determine the maximum grounded ice extent and ice retreat rate for the east-central Ross Sea by completing sedimentological analyses and by radiocarbon dating sediments that mark the transition from glacial to postglacial conditions. Presently, few data constrain the chronology of ice retreat and the extent of glacial ice during marine isotope stage 2 in the east-central Ross Sea. We are reporting preliminary results in which we present characteristics of

two glacial marine diamictos of different ages from the western Ross Sea and then relate cores from the east-central Ross Sea to them. Although the east-central Ross Sea sediments are being dated, the results are not yet available.

Core *NBP9501-39*, from the western Ross Sea (figure 1), contains a 2-meter (m) thick diatomaceous mud unit underlain by a last-glacial-maximum-age massive diamicton interpreted as glacial marine. The core site is located 2–3 kilometers north of a bathymetric high interpreted as a grounding line deposit (Shipp and Anderson 1994). The diamicton unit from *NBP9501-39* has been identified in the 3.5-kilohertz (kHz) seismic record and is 6–8 m thick; only the upper 0.5 m

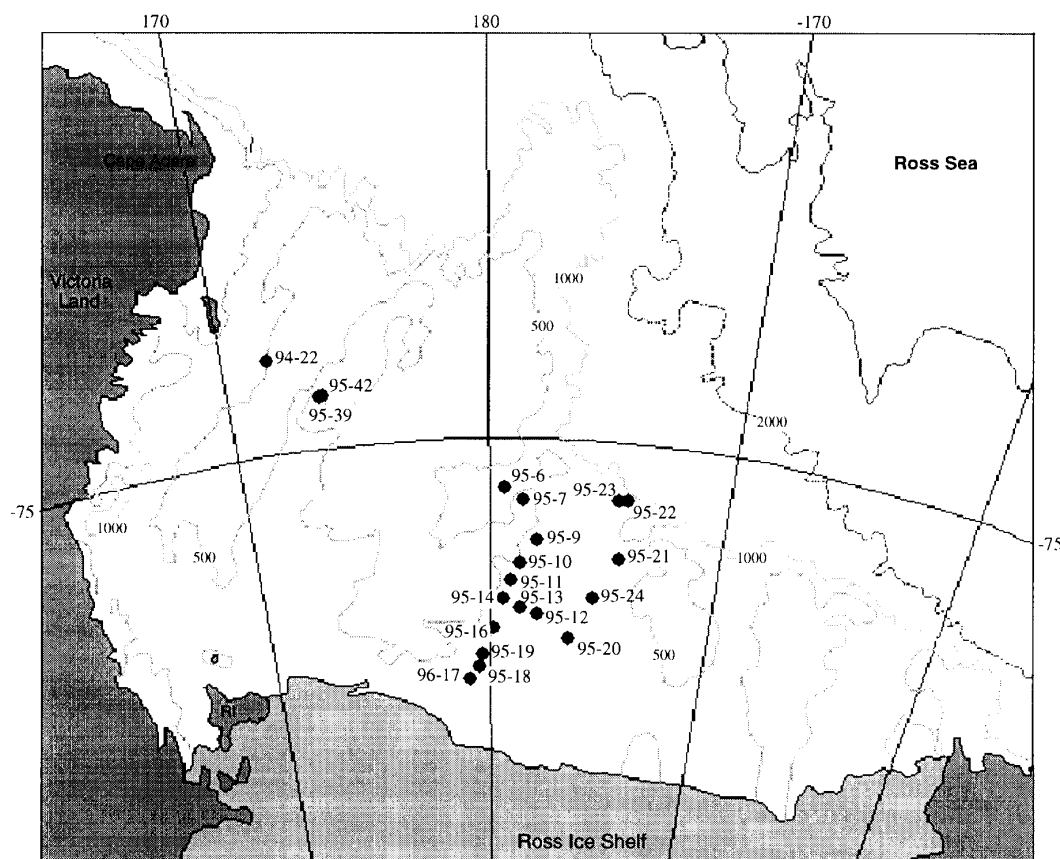


Figure 1. Map of the Ross Sea showing sediment core locations.

of the acoustic unit was sampled by core 39. This acoustic unit can be traced northward to piston core *NBP9501-42* (figure 1), which is primarily composed of a massive diamicton containing abundant foraminifera that are last glacial maximum in age. A radiocarbon date on foraminifera from the massive diamicton in core 39 is last glacial maximum in age; therefore, the upper part of the 6–8-m thick acoustic unit was deposited during the early part of marine isotope stage 2. The last-glacial-maximum-age glacial marine diamictons from the western Ross Sea outer continental shelf identified in previous studies (Licht 1995; Licht et al. 1996) are probably equivalent to this acoustic unit identified in the 3.5-kHz data.

Core *NBP94-1-22* is also located slightly beyond the grounding line in the western Ross Sea (figure 1) and is a massive diamicton that grades upward into a Holocene-age stratified diamicton containing 1–5-centimeter (cm) thick layers of pebble-rich diatomaceous mud (figure 2). The diatomaceous mud layers resulted from periods of seasonally ice-free waters or upwelling, nutrient-rich water at this site. Radiocarbon dates on bulk organic carbon range from 7.5 to 8.5 ¹⁴C in the upper 85 cm of the core (table). Sedimentation rates range from 8 cm per 100 years to 20 cm per 100 years in this interval. The high rates of sedimentation may be a function of rapid ice-sheet retreat or a function of ocean circulation controlling the distribution of ice-rafted debris and surface productivity. The rapid sedimentation at 8,500 years ago can be attributed to activity of

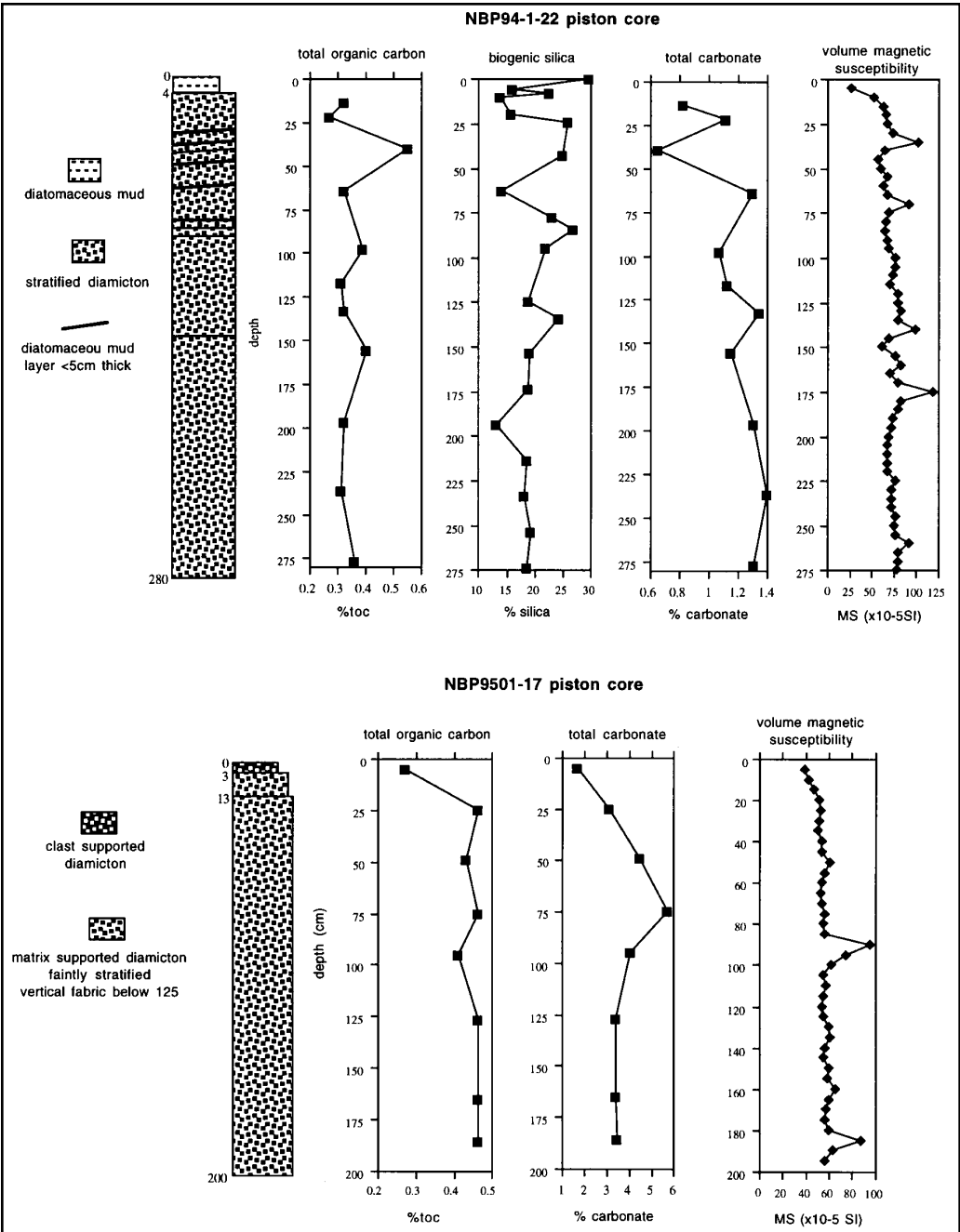


Figure 2. Sedimentological analyses from two Ross Sea piston cores. *NBP94-1-22* is located in the western Ross Sea and core *NBP9501-17* is located in the east-central Ross Sea.

New radiocarbon dates from the Ross Sea

Lab number ^a	Core	Depth (cm)	Uncorrected	Corrected	Material
AA19910	<i>NBP94-1-22</i>	2–4	8,880±75	7,680	Bulk organic carbon ^b
AA19911	<i>NBP94-1-22</i>	42–43.5	9,435±75	8,235	Bulk organic carbon ^b
AA19921	<i>NBP94-1-22</i>	83–35	9,615±75	8,415	Bulk organic carbon ^b

^aUniversity of Arizona, Tucson ^bDecalcified

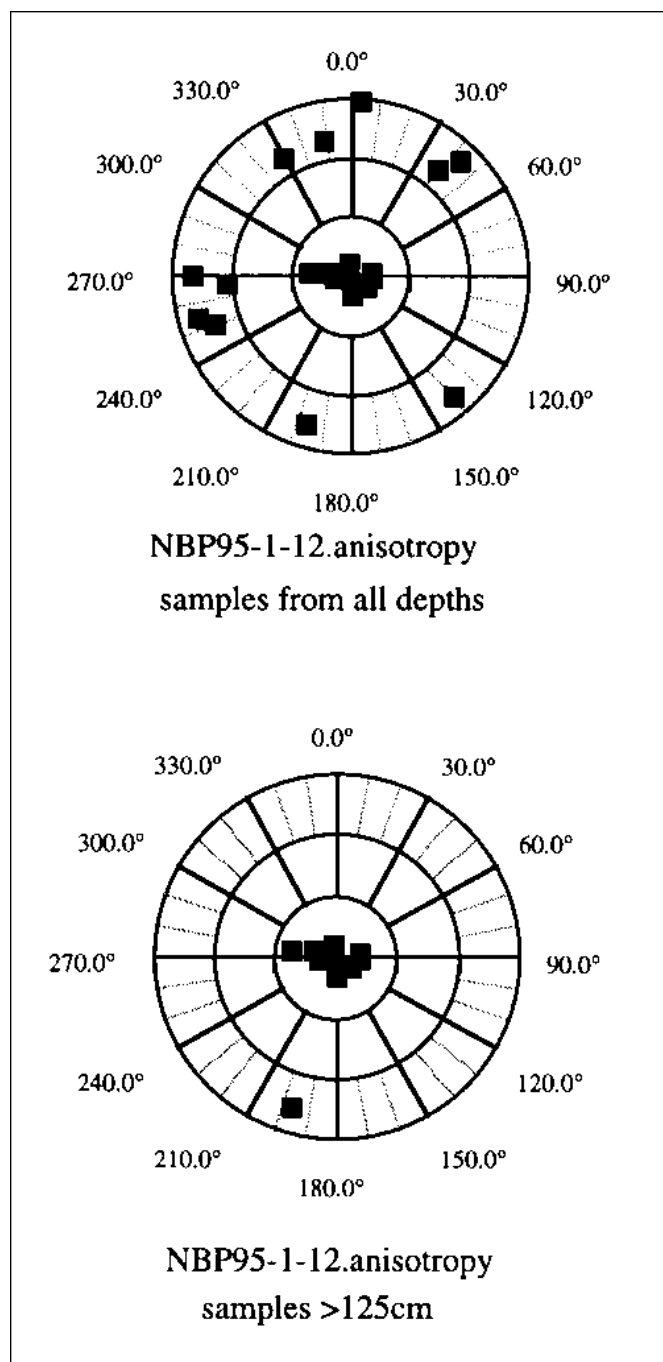


Figure 3. Stereographic projection of anisotropy of magnetic susceptibility data showing that the long axes of fine-grained sediment in a massive diamicton are oriented vertically below 125 cm in core NBP9501-12.

the west antarctic ice sheet because the westernmost Ross Sea, at least to Drygalski Ice Tongue (ice stream trough A), was free of grounded glacial ice by 10,000 to 11,000 years ago (Domack, Shipp, and Jacobson 1996; Licht et al. 1996).

East-central Ross Sea piston cores generally contain a massive diamicton as the basal unit overlain by a stratified diamicton. Approximately 50 percent of the massive basal diamictons have a vertical pebble and fine-grained sediment fabric that is evident in x-radiographs and anisotropy of susceptibility data (figure 3). In the upper diamicton, 70 percent of the cores have slight to strong stratification. Radiocarbon ages of these stratified diamictons are pending and sedimentological analyses of both units are underway (figure 2). These preliminary results allow us to speculate on the relationship between the western Ross Sea cores and the east-central Ross Sea cores.

We propose two possible scenarios to relate the stratified diamictons from the east-central Ross Sea to those from the western Ross Sea:

- if the east-central Ross Sea stratified diamictons are of last-glacial-maximum age, then the sediment would be equivalent to the glacial marine diamicton in the base of NBP9501-39 and would indicate that grounded ice did not reach the continental shelf edge in the east-central Ross Sea during the last glacial maximum, or
- if the age of the base of the stratified diamictons is Holocene (or postglacial), it will provide the timing of ice retreat across the continental shelf, and the sediment would be equivalent to the rapidly deposited stratified diamicton in NBP94-1-22.

This research was supported by National Science Foundation grant OPP 91-17958. We are grateful to the Florida State Antarctic Research Facility for their assistance.

References

- Bindshadler, R.A. (Ed.). 1995. *WAIS: The West Antarctic Ice Sheet Initiative: A multidisciplinary study of rapid climate change and future sea level* (Conference publication). Arlington, Virginia: National Science Foundation.
- Domack, E.W., S. Shipp, and E. Jacobson. 1996. Recessional rates of the west antarctic ice sheet in the western Ross Sea. Abstracts volume of 4th Annual West Antarctic Ice Sheet Initiative Science Workshop, 6-7 September 1996.
- Licht, K.J. 1995. Marine sedimentary record of ice extent and Late Wisconsin deglaciation in the western Ross Sea, Antarctica. (M.S. thesis, University of Colorado, Boulder, Colorado.)
- Licht, K.J., N. Dunbar, A.E. Jennings, and J.T. Andrews. In press. Sedimentological evidence for the maximum extent of grounded ice in the western Ross Sea during the last glacial maximum. *Geological Society of America Bulletin*.
- Licht, K.J., A.E. Jennings, J.T. Andrews, and K.M. Williams. 1996. Chronology of late Wisconsin ice retreat from the western Ross Sea, Antarctica. *Geology*, 24(3), 223-226.
- Shipp, S.S., and J.B. Anderson. 1994. Late Pleistocene deglaciation of Ross Sea Antarctica inferred from high-resolution seismic data. *Geological Society of America Abstracts with Programs*, 26(7), A-364.

Hydrothermal and hydrographic surveys of the Bransfield Strait: Results from cruise *NBP95-07*

GARY P. KLINKHAMMER, CAROL S. CHIN, and CARA WILSON, *College of Oceanic and Atmospheric Sciences, Oregon State University, Corvallis, Oregon 97331-5503*

LAWRENCE A. LAWVER, *Institute for Geophysics, University of Texas at Austin, Austin, Texas 78759-8397*

The Bransfield Strait is a narrow marginal basin separating the South Shetland Islands from the Antarctic Peninsula. It consists of three subbasins: the Eastern, Central, and Western Bransfield Basins (figure 1). The strait was formed by the rifting of a volcanic arc.

In November 1995, we surveyed 340 kilometers (km) of the Bransfield Strait for hydrothermal activity, using a station spacing of approximately 20 km. We conducted 32 deployments of the ZAPS (Zero-Angle Photon Spectrometer; Klinkhammer 1994) sled instrument package. We also carried out an additional 12 conductivity-temperature-depth (CTD) rosette casts to collect larger volumes of sea water. The Central

Basin (figure 1) was the focus of most of the detailed work, but seven operations were carried out in the Eastern Basin.

Data collection

The most cost-effective and efficient method of searching for hydrothermal sources on the seafloor is the detection of hydrothermal plumes in the water column. This approach not only identifies individual vent fields but also places the hydrothermal activity in a regional hydrographic context. Characterization of the water column is important because knowledge of the background stratification is critical to interpreting plume data.

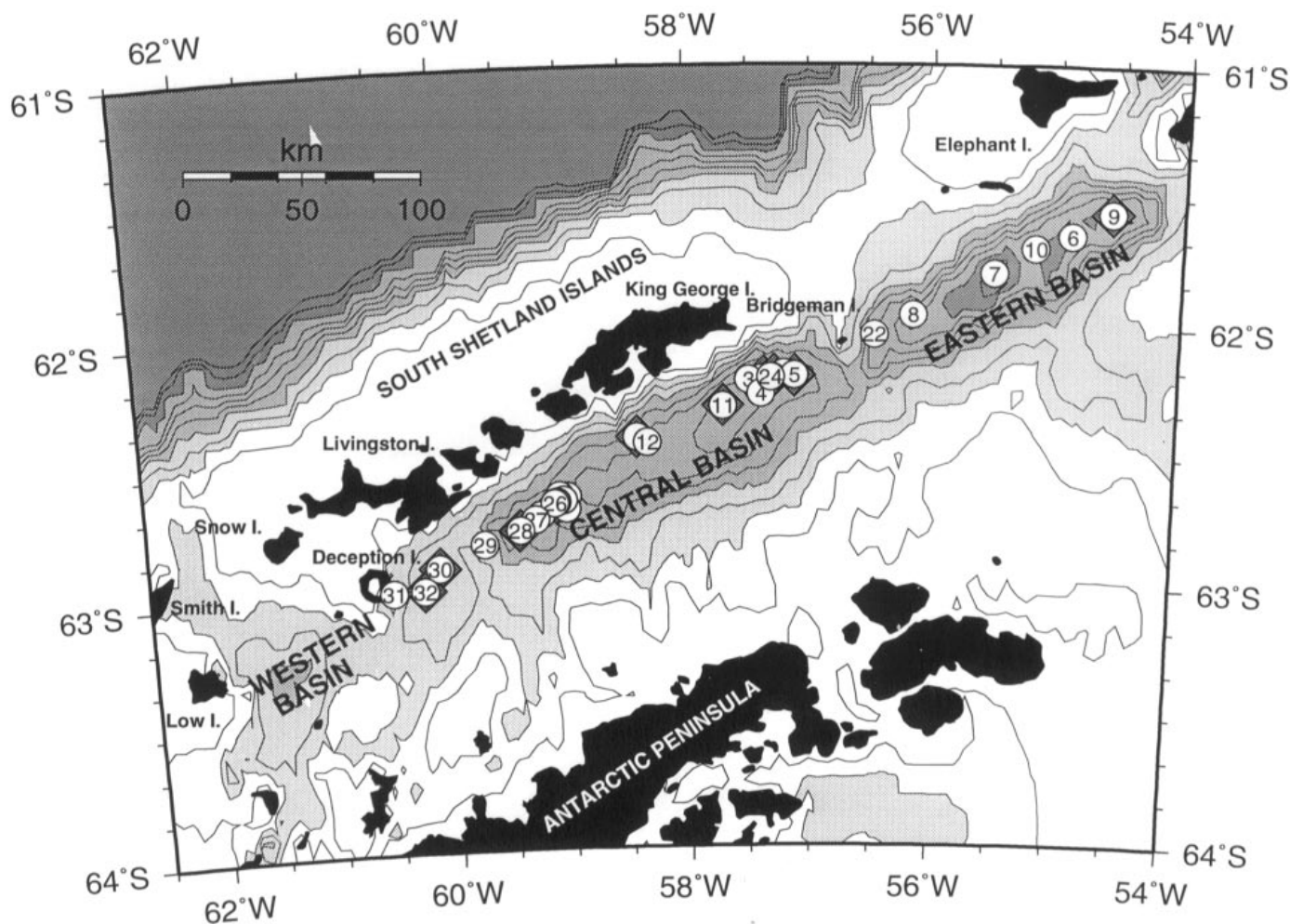


Figure 1. Location map showing the Bransfield Strait between the Antarctic Peninsula and the South Shetland Islands. The circles denote the locations of sled deployments, and the diamonds indicate the locations of rosette casts. Depths greater than 500 m are shaded; degrees of shading change at 1,000 m and 2,000 m.

The ZAPS instrument package consists of the following:

- a SeaBird 9/11 plus CTD,
- a rosette fitted with six 1.2-liter Niskins,
- a SeaTech transmissometer,
- a Chelsea nephelometer,
- a SeaTech light scattering sensor,
- a Sea Point turbidity sensor, and
- the ZAPS probe which measures dissolved manganese *in situ*.

Water samples for onshore analysis were collected using this package as well as the ship's CTD/rosette.

A three-step approach was used in surveying the strait, looking at increasingly smaller areas to pinpoint the sources of the hydrothermal plumes observed. This survey approach located three major venting areas in the Central Basin. Because of time constraints, only the first phase of this survey strategy was completed in the Eastern Basin. Although hydrothermal activity was indicated by some of the signals we observed in this basin, the plume sources were not identified.

Laboratory analyses

- *Manganese analyses.* Manganese determinations with the ZAPS fiber optic spectrometer were calibrated by running standard solutions onshore before the field operations. These calibrations were adjusted after the cruise by comparing the field data to the manganese concentrations in samples collected from the sled's rosette. These samples were analyzed for dissolved manganese and total dissolvable manganese (Klinkhammer, Weiss, and Bender 1977) using a Fisons VG PlasmaQuad II Plus ICPMS interfaced to a Dionex Chelation Concentration Module.
- *Helium analyses.* Over 100 water samples were collected for helium isotopic analysis. D. Graham and J. Lupton conducted these analyses at the National Oceanic and Atmospheric Administration facility in Newport, Oregon.

Hydrothermal activity

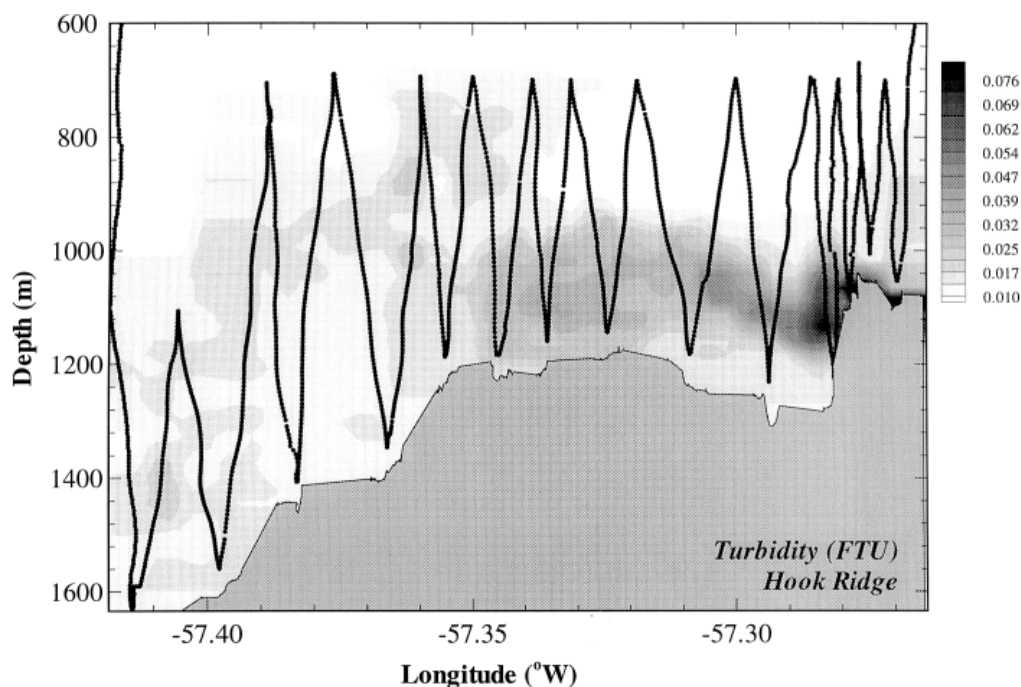
Every major volcanic structure in both the Central and Eastern Basins was surveyed, and evidence of hydrothermal activity was found in both basins. The strongest signals were observed in the Central Basin (figure 1) along Hook Ridge (SL24), the Middle Ridge of the Three Sisters (SL26), and the Little Volcano (SL27). Anomalously high manganese concentrations [up to 13 nanomolar (nM), background of 4 nM] and $\delta^3\text{He}$ of 38 percent (background of 2 percent) were observed over Hook Ridge, where strong particle anomalies were also detected (figure 2). In addition, temperature anomalies between 0.010 and 0.025°C were measured in these areas.

Hydrothermal activity occurs along a linear but discontinuous neovolcanic ridge that runs between Deception Island and Bridgeman Island in the Central Basin and continues northeast of Bridgeman Island in the Eastern Basin. The rise heights of the plumes [200–300 meters (m)] and the abundance of hydrothermally derived particles indicate that the vents' fluids are high temperature and iron rich. We also found evidence of hydrothermal discharge from the mouth of Deception Island, a submerged caldera. The injection of this plume of turbid and probably metal- and nutrient-rich water into the surface waters of the western Central Basin has biogeochemical implications for productivity in this region of high biological activity.

Hydrography

A secondary objective of this work was to produce a detailed hydrographic cross-section of water in the Bransfield Strait. The unique hydrography of the Bransfield Strait has been of interest to oceanographers since the turn of the century (Clowes 1934). The Central and Eastern Basins are isolated below 500 m (see figure 1), and the deep water within the strait is considerably colder and fresher than water at similar depths

Figure 2. Vertical section of nephels (FTU, formazine turbidity units) from southwest to northeast along Hook Ridge, southwest of Bridgeman Island. Darker shading indicates higher concentrations of hydrothermally derived particles. Hydrothermal manganese and helium-3 anomalies were also observed in this area (see text). The sawtooth line is the path of the instrument package as it was towed from along the ridge.



outside the strait in the Weddell Sea or the Drake Passage (Clowes 1934; Gordon and Nowlin 1978). As seen in figure 3, the deep water in the Eastern Basin is warmer than the shallower bottom water within the Central Basin, indicating that multiple processes are at work in the deep-water formation of the strait. Results from *NBP95-07* have shown that the Eastern Basin has a much more complex hydrography than the Central Basin. One of the factors contributing to the structure of the deep Eastern Basin water is the overspilling of Central Basin water, evident on figure 3 as the cold pool of water at 56.5°W.

Conclusions

We discovered three active hydrothermal sites in the Bransfield Strait, all of which appear to contain high-temperature, black smoker type vents that produce iron-rich fluids. We also found evidence of active vent sites in the Eastern Basin though we did not locate the vents.

Because of the relative isolation of the Bransfield Strait from another hydrothermal area or the global mid-ocean ridge system, its discovery raises many questions for future research ranging from the biogeographical distribution of vent fauna to the relationship between spreading rate, crustal production, and hydrothermal activity.

We acknowledge the support of Captain Joe Borkowski and crew of the *Nathaniel B. Palmer* as well as Jim Holik, the Marine Project Coordinator, and the rest of the Antarctic Support Associates personnel. In addition, this work benefit-

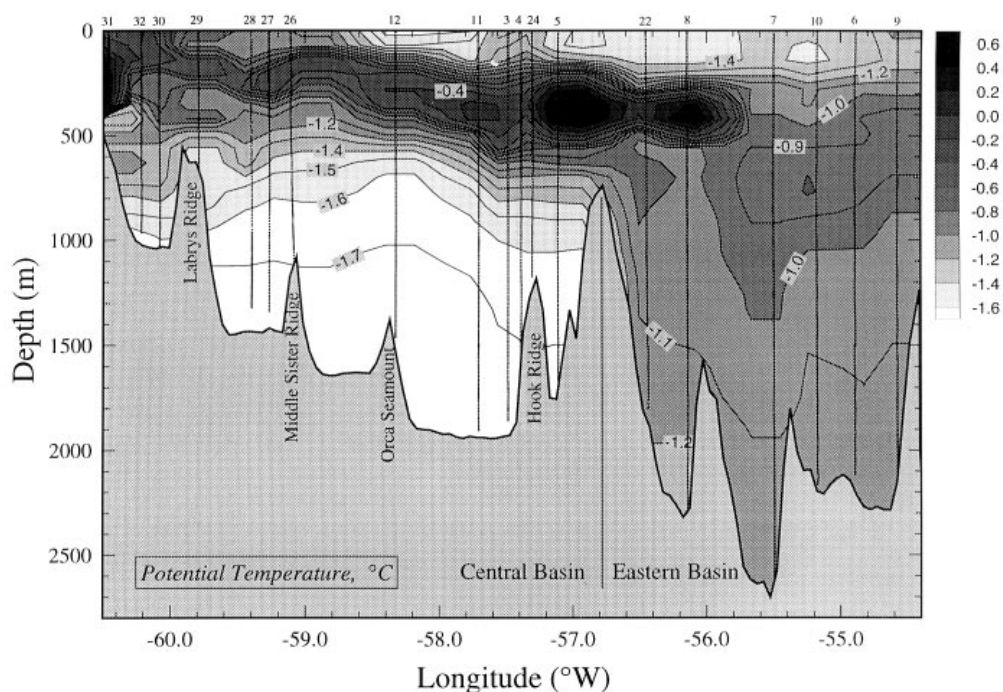


Figure 3. Potential temperature section through the Central and Eastern Basins. The 1,000-m sill near Bridgeman Island separates the two basins, and midwaters from the Central Basin occasionally spill over to the Eastern Basin, as seen from the cold (below -1.2°C) pool of water at 56.5°W.

ed from the assistance of the other scientists on *NBP95-07*. This research was funded by National Science Foundation grant OPP 93-17361 to G.P. Klinkhammer.

References

- Clowes, A.J. 1934. Hydrology of the Bransfield Strait, *Discovery Reports*, 9, 1-64.
- Gordon, A.L., and W.D.J. Nowlin. 1978. The basin waters of the Bransfield Strait, *Journal of Physical Oceanography*, 8(2), 258-264.
- Klinkhammer, G.P. 1994. Fiber optic spectrometers for *in situ* measurements in the oceans: The ZAPS probe, *Marine Chemistry*, 47, 13-20.
- Klinkhammer, G.P., R.F. Weiss, and M.L. Bender. 1977. Hydrothermal manganese in the Galapagos Rift, *Nature*, 269, 319-320.

Analysis of laminated antarctic marine sediments

AMY LEVENTER and LORA STEVENS, *Limnological Research Center, University of Minnesota, Minneapolis, Minnesota 55455*

Analysis of varved lacustrine sediments has been instrumental in the development of high-resolution paleoclimate records from terrestrial sites. The preservation of sediment layers, which record seasonal and annual events, occurs in a limited number of settings, and far fewer marine records have been analyzed to date. Reports of laminated sediments from the Antarctic date back to the 1970s, but

detailed analysis of the laminae and an assessment of the processes that form the layers have not been done. The primary objective of this project was to examine microscopically all antarctic downcore sediments that previously have been described as laminated in the "Sediment Description" books compiled by the Antarctic Marine Geology Research Facility at Florida State University. Our goal was to determine

whether any of the laminations could be varves, representing annual deposition.

So far, 46 sections of 19 cores have been examined (table). Sediment samples were collected from the cores in rectangular aluminum boxes, which protected them during transport. Prior to embedding, the samples were removed from these boxes and arranged in sets of seven in Rubbermaid® food-storage trays. Each tray was then photographed with 35-mm film for archival purposes and x-rayed. Embedding was done following the technique of Card (1994). The samples were braced with packing foam to reduce erosion of the sample edges and dehydrated by liquid-acetone exchange. Exchanges were made every 12 hours until the water content of the sediment was less than 0.5 percent. The number of exchanges necessary varied according to sediment type; diatomaceous ooze took less time than clay-rich hemipelagic sediment. Once the samples were dehydrated, the foam was removed and the sediment was covered with Spurr's® epoxy, which has a refractive index of 1.54. Because excess acetone prevents the epoxy from setting properly, 10 epoxy exchanges at 12-hour intervals were made to ensure complete removal of the acetone. After the final exchange, the trays were filled to the level of the sample tops and allowed to harden for 2 weeks at room temperature. The trays were then cured in a drying oven at 50°C for 3 days. The samples were cut from the epoxy blocks and trimmed to the dimensions of standard petrographic thin-section using a diamond-blade trim saw. They were also notched to indicate stratigraphic up. Finally, covered thin sections were made.

In many cases, what had been described as laminated was seen in thin section as a single discrete layer, most likely indicating a single event. In general, these layers were composed of nearly monospecific diatom assemblages. Genera and species present include *Rhizosolenia* spp., *Chaetoceros* spp., and *Corethron criophilum*, all previously noted in layers from both the Ross Sea and Antarctic Peninsula (Jordan et al. 1991; Leventer et al. 1993, in press). Similar morphologic features of these groups (slender structures, long setae or spines) suggest a physical mechanism for aggregation and mass sedimentation, resulting in the presence of a fairly uniform layer in the sediments.

Two other types of laminations were observed, however. In sediments from the continental slope off the George V Coast, alternating layers of subrounded quartz, most likely of aeolian origin, and organic debris were observed (figure 1). The laminae are of millimeter scale in thickness, and the quartz grains range from approximately 20 to 50 microns (µm) in diameter. In general, the quartz grains are not a mixture but are size-sorted, and laminae contain either larger or smaller grains. These layers may represent a seasonal succession of lithogenic and biogenic flux. At the time of initial sea-ice breakout, ice-rafted debris (originally of aeolian origin) may be released to the water column. Following ice breakout, open-water primary production results in the delivery of organic material to the ocean. The organic layers in the sediment may be the degraded products of phytoplankton blooms.

The second type of layering observed was from sediments of the Palmer Deep, a basin approximately 20 kilometers south

Thin sections from antarctic marine sediments

Core	Latitude (°S)	Longitude	Water depth (m)	Subsample depth (cm)
DF79-1	65.48	141.5°E	2,022	23–29 110–114.5 130.5–137.8
DF79-12	66.57	141.53°E	228	104.5–109.5 124.2–130.2 192–198
DF79-13	66.32	143.32°E	807	406.2–409.2 512–520
DF79-19	65.78	145.2°E	2,598	47–57 254–260 267–275
DF79-56	65.7	146.52°E	1,235	32–37.2
DF80-2	70.87	168.82°E	1,079	22–29 32.5–39.5 87–94 332–339
DF80-30	69.52	165.95°E	2,094	350.5–357.5 360–374
DF80-31	69.8	166.38°E	1,676	150–158
DF81-18	63.52	61.57°W	1,298	137–144 196.5–205.5 221–226
DF82-34	62.3	57.62°W	1,979	410–417
DF82-182	63.86	57.51°W	405	51–58 92.4–99.4
DF82-197	63.72	57.23°W	750	32.1–39.1
DF86-4	62.2	54.78°W	658	153.5–159
PD88-3-22	64.83	62.65°W	440	92.5–99.5 44.2–49.6 676.5–679
PD88-3-150	64.28	60.99°W	440	442–449
PD89-4-3	62.24	57.48°W	1,989	228.5–236
PD89-4-4	62.32	57.66°W	1,997	162–167 228–235.5
PD92-26	63.89	61.49°W	1,130	97.5–104.5 591–598
PD92-30	64.86	64.21°W	1,040	88–96.4 96.5–104 191.5–198.5 185–191 203–209 483–491 473–481 462–468.2 727–735 735–742

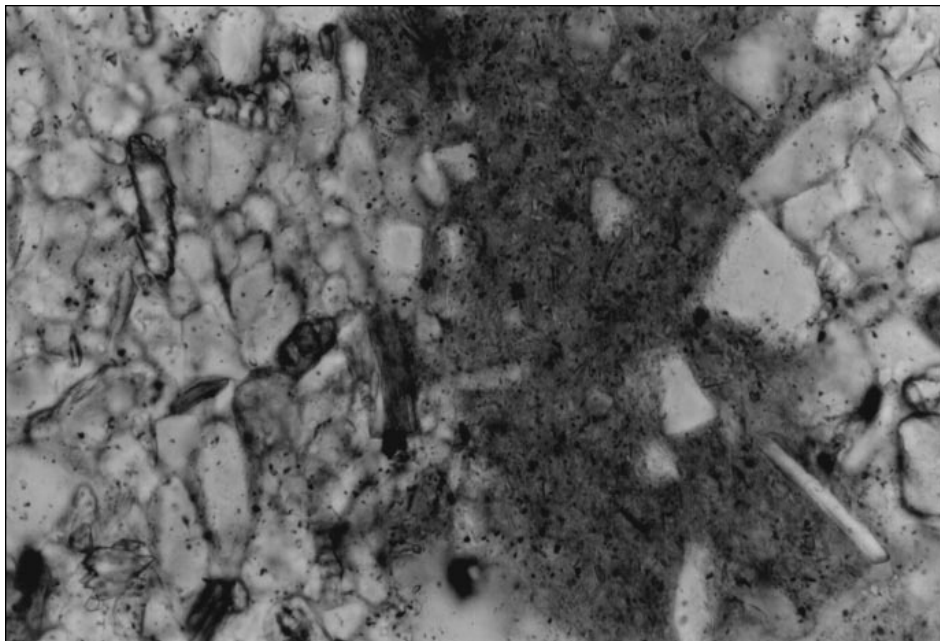


Figure 1. Sedimentary layers from core DF79-56, from the George V Coast. Note the distinct layers: quartz grains on either side of dark, amorphous organic debris. For scale, the photo is 310 μ m across.

of Anvers Island. Core PD92-30, from the basin, has already been analyzed in detail and demonstrates approximately 200-year cycles of paleoproductivity (Leventer et al. in press). Periods of high primary productivity are distinguished lithologically from other sections of the core by the presence of millimeter-scale laminations. In thin section, it is apparent that individual laminae represent blooms of different species of diatoms, including *Thalassiosira antarctica*, *Rhizosolenia* spp.,

Corethron criophilum, *Coscinodiscus bouvet*, *Thalassiothrix* sp?, and *Chaetoceros* spp. (figure 2). In many cases, layers dominated by *Chaetoceros* vegetative cells alternate with those dominated by *Chaetoceros* resting spores. This sequence suggests a seasonal succession of vegetative cells which undergo spore formation in the late stages of a phytoplankton bloom (Leventer 1991). More detailed laminae counts and laminae thickness measurements must be done to determine the full history of high-productivity periods, which have periodically characterized this region.

This research was supported by National Science Foundation grant OPP 89-17200 and National Oceanic and Atmospheric Administration grant NA 36GP0817.

References

- Card, V.M. 1994. Diatom communities, ice-out, and varve formation in Minnesota lakes. (Doctoral dissertation, University of Minnesota.)
- Jordan, R.W., J. Priddle, C.J. Pudsey, P.F. Barker, and M.J. Whitehouse. 1991. Unusual diatom layers in Upper Pleistocene sediments from the northern Weddell Sea. *Deep-Sea Research*, 38(7), 829-843.
- Leventer, A. 1991. Sediment trap diatom assemblages from the northern Antarctic Peninsula region. *Deep-Sea Research*, 38(8/9A), 1127-1143.
- Leventer, A., E.W. Domack, S. Ishman, S. Brachfeld, C. McClennen, and P. Manley. In press. 200-300 year productivity cycles in the Antarctic Peninsula region: Understanding linkages among the sun, atmosphere, oceans, sea ice and biota. *Geological Society of America Bulletin*.
- Leventer, A., R.B. Dunbar, and D.J. DeMaster. 1993. Diatom evidence for late Holocene climatic events in Granite Harbor, Antarctica. *Paleoceanography*, 8, 373-386.

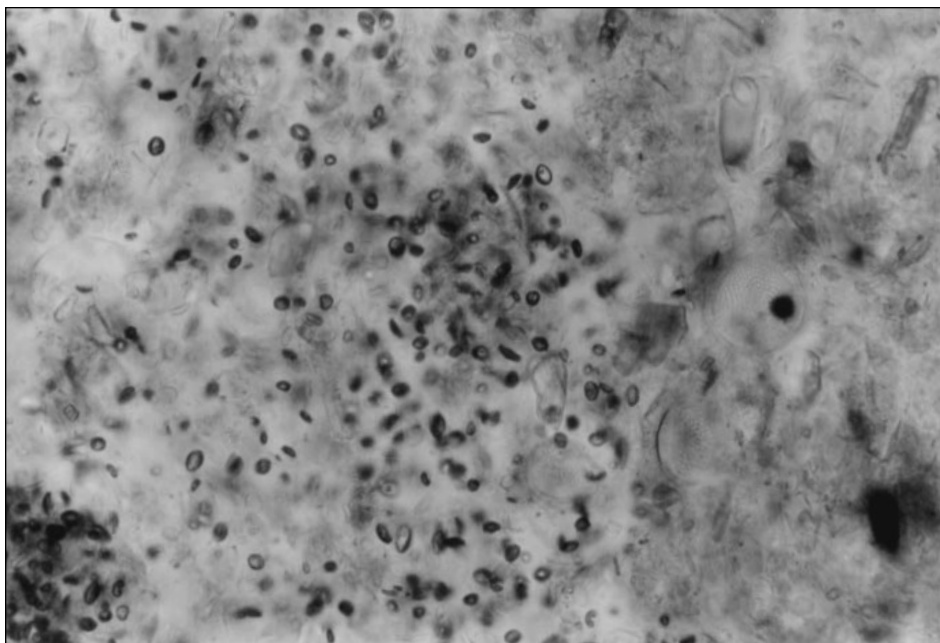


Figure 2. Sedimentary layers from core PD92-30, from the Palmer Deep. Note the band of *Chaetoceros* resting spores in the center of the photograph. To the left, the assemblage is dominated by *Chaetoceros* vegetative cells. To the right are specimens of the open water species *Thalassiosira*. Scale is 310 μ m across.

Porewater chemistry of Ross Sea diamictons: A till or not a till?

TODD W. RAYNE and EUGENE W. DOMACK, *Department of Geology, Hamilton College, Clinton, New York 13323*

As part of our investigation into the glacial history of the west antarctic ice sheet, we collected a number of piston cores in February 1995 using the R/V *Nathaniel B. Palmer*. Many of these cores recovered a structureless diamicton (a poorly sorted sediment). This unit has since proved to be the basal interval in a complex suite of sediment layers. Traditional interpretations of this diamicton have held it to be a till deposited beneath the once expanded west antarctic ice sheet. The water content (20–30 percent) and textural properties are suggestive of such an origin. To test this hypothesis for the genesis of the diamicton, we extracted pore waters from the sediment onboard the ship and later analyzed the water for its chemistry. This article outlines our methods and assumptions regarding the porewater evolution of the sediment. Briefly, if the diamicton were indeed deposited as a lodgement till beneath the west antarctic ice sheet, then it should (theoretically) retain a meltwater signature consistent with a subglacial origin. If on the other hand the sediment was deposited in a subaqueous marine setting, the diamicton should retain waters of marine origin.

We squeezed 33 samples of diamicton from 15 separate diamicton cores using a modified Reeburgh device (figure 1; Reeburgh 1967). Water was collected in small glass vials and procedures were followed to prevent and assess evaporation of water after collection. We carved sections of diamicton approximately 10 centimeters (cm) long from freshly cut cores and removed surface sediment, which was in contact with the core liner. Squeeze times ranged from 3 to 8 hours for some samples because of the impermeable nature and low water content of the sediment. Water samples were transported to Hamilton College. Several months after collection, the water samples were analyzed for the chloride ion concentration (Cl^-) using ion chromatography at Oneida Research

Services, Inc. Analyses were conducted using a Dionex 4000i series ion chromatography system. A calibration curve was generated using standards that ranged from 10 to 500 parts per million. Samples were therefore diluted by 50:1 to keep the results within the calibration curve. Results ranged from 17.6 to 23.4 parts per thousand (ppt). The mean Cl^- was 20.54 ppt with a low standard deviation of 0.085. Results versus core depth are illustrated in figure 2.

Because Cl^- is not adsorbed by solid phases in the sediment, and because it diffuses very slowly in an impermeable sediment, it traces the movement of sea water over time within sediments that would have originated with fresh pore water, such as tills observed at Upstream B (Kamb personal communication). If a lodgement till was deposited from marine-based ice, then upon glacial recession and exposure at or near the seafloor, the till should slowly equilibrate with respect to its Cl^- concentration and sea water. Because diffusion processes are time dependent, such migration of Cl^- should also serve as a chronometer for the age of marine incursion if the diffusion coefficient is well known.

The movement of dissolved substances in the direction of their concentration gradient is called "diffusion." The mass of a diffusing substance is proportional to the concentration gradient and is known as Fick's first law. Fick's first law and the equation of continuity can be combined to yield Fick's second law, which relates the concentration of the substance



Figure 1. Photograph of undergraduate student Martin Hilfinger aboard the R/V *Nathaniel B. Palmer* using sediment pore water device to extract water from diamicton samples.

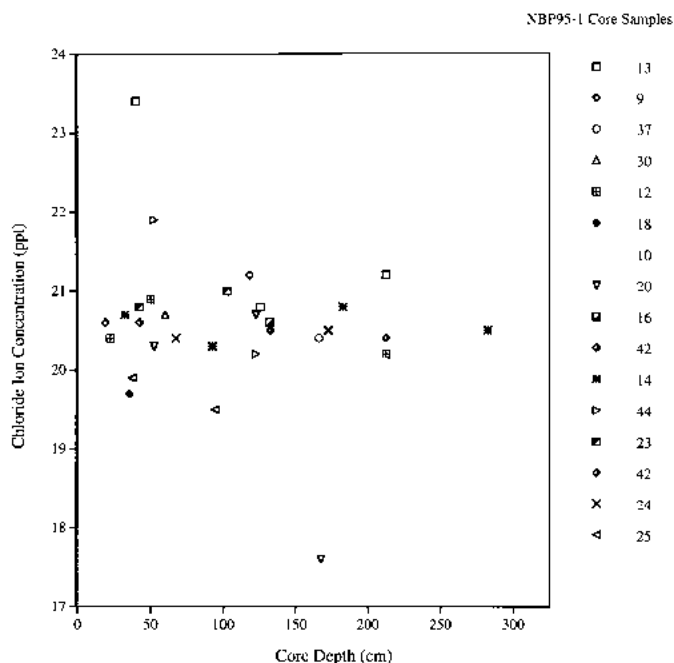


Figure 2. Plot of chloride ion concentration versus depth in a number of diamicton cores collected in the Ross Sea during cruise NBP95-1. Symbols represent different cores. (C/Co denotes carbon/cobalt.)

to space and time. In one dimension, the analytical solution to Fick's second law is (Crank 1956):

$$C_i(x,t) = C_o \operatorname{erfc}[x / 2\sqrt{D^*t}] \quad (1)$$

where C is concentration, x is distance, t is time, D^* is the apparent diffusion coefficient for porous media, and erfc is the complimentary error function.

The apparent diffusion coefficient is the product of the aqueous diffusion coefficient and an empirical coefficient, less than 1, that is related to tortuosity. Aqueous diffusion coefficients are well known for electrolytes in aqueous solutions. For example, the aqueous diffusion coefficient for Cl^- in water at 25°C is 20.3×10^{-6} square centimeters per second (Li and Gregory 1974). The tortuosity coefficient is a function of the grain size, shape, and sorting of the porous medium. Freeze and Cherry (1979) report a range of values from 0.01 to 0.5 from laboratory studies. Higher values are associated with less tortuous pathways.

This study used equation 1 to simulate the one-dimensional movement of chloride ions through diamicton. Different values of the tortuosity coefficient were used to examine the amount of time for chloride to diffuse through a 2-meter thickness of diamicton. Boundary values were 19 ppt and 0 ppt. (See figure 3.)

Results of simulations demonstrate that diffusion is a very slow process. Using the highest tortuosity coefficient, concentrations at the outlet boundary did not reach 19 ppt until nearly 50,000 years. Using lower tortuosity coefficients that are more realistic for the poorly sorted diamicton, concentrations at the outlet boundary don't reach 19 ppt after 100,000 years.

These results demonstrate that the diamictons are glacial marine sediments or are lodgement tills that are in excess of 100,000 years old. Hence, if recent lodgement tills exist on the floor of the Ross Sea, then they must lie at depths greater than those penetrated by our cores. It should be noted that the morphology of the Ross Sea bottom and seismic reflection data all suggest a glaciated substrate. Chloride ion concentrations have not been systematically studied within glaciated continental margins. Data from Prydz Bay (Chambers 1991, pp. 375–392) suggest some penetration of meteoric waters at near-coastal sites but otherwise indicate normal marine salinities for

the thick glacial and glacial marine diamictons recovered on this shelf. Sampling was very limited, however, because of poor recovery and most samples were obtained at depths greater than 100 meters below the seafloor (Chambers 1991, pp. 375–392). Our results show marine salinities very close to the seafloor. Hence, the lodgement tills, if they exist on the Ross Sea continental shelf, may lie at depths greater than 10 meters. The other possibility is that depositional processes across the shelf during glacial maximum are dominated by complete reworking of marine sediments with little addition of fresh (glacial) water during redeposition; a process different from that observed at Upstream B today.

This work was supported by National Science Foundation grant OPP 91-18462 to Hamilton College. We thank the crew of the R/V *Nathaniel B. Palmer* and support personnel from Antarctic Support Associates for all their help during cruise 95-1. Martin Hilfinger assisted with shipboard sampling for this project and his help was greatly appreciated.

References

- Chambers, S.R. 1991. Solute distributions and stable isotopic chemistry of interstitial waters from Prydz Bay, Antarctica. In Y. Barron, B. Larsen, et al. (Eds.), *Scientific results of the Ocean Drilling Program* (Vol. 119). College Station, Texas: Ocean Drilling Program.
- Crank, J. 1956. *The mathematics of diffusion*. New York: Oxford University Press.
- Freeze, R.A., and J.A. Cherry. 1979. *Groundwater*. Englewood Cliffs, N.J.: Prentice-Hall.
- Kamb, B. 1995. Personal communication.
- Li, Y.-H., and S. Gregory. 1974. Diffusion of ions in sea water and in deep-sea sediments. *Geochimica et Cosmochimica Acta*, 38, 703–714.
- Reeburgh, W.S. 1967. An improved interstitial water sampler. *Limnology and Oceanography*, 12, 163–165.

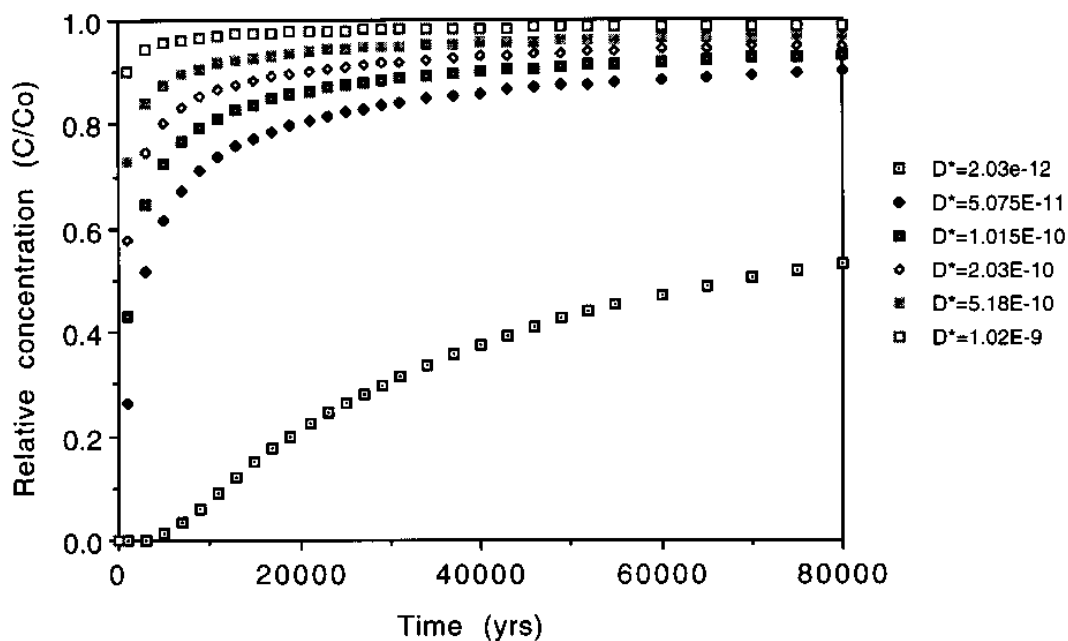


Figure 3. Breakthrough curve at 2.0 meters depth for chloride using different diffusion factors (D^*). Concentrations are relative to 19 ppt.

Bulk salinity characteristics of first-year sea ice in the Pacific sector of the southern oceans

TED MAKSYM and M.O. JEFFRIES, *Geophysical Institute, University of Alaska, Fairbanks, Alaska 99775-7320*

The salinity characteristics of antarctic sea ice are determined by a complex interaction of factors, including thermodynamic growth rates, sea-water salinity, deformational events, bottom ablation, and surface flooding and snow-ice formation. Regional variations in the nature and timing of these events can be manifested in regional variability of sea-ice bulk salinity.

As part of four sea-ice research cruises aboard the R/V *Nathaniel B. Palmer* in the austral winters of 1993, 1994, and 1995, salinity profiles were determined for a total of 342 ice cores from the Ross, Amundsen, and Bellingshausen Seas. The ice floe sampling sites are shown in figure 1 for each cruise. The salinity profiles were generally S-shaped (Eicken 1992), having a high surface salinity, averaging 10.3 parts per thousand (ppt) in the top 5 centimeters (cm), and dropping to about 6 ppt in the lower parts of the ice sheet. The high surface salinity can be attributed to flooding of the ice surface with sea water and the subsequent formation of snow ice (Eicken 1992), as evidenced by the high proportion of snow ice identified in the cores (Jeffries unpublished data).

Figure 2 shows bulk ice salinity versus core length for each of the four cruises. Although these values are in general agreement with values for the Arctic, the data show considerable scatter, particularly for the early winter 1995 cruise. This scatter is likely due to the variety of processes that affect sea-ice salinity in this region, in contrast to the less complicated growth regime predominant in the Arctic.

Of note, however, is that for core lengths between about 40 and 100 cm, the bulk salinity values for the 93-5, 94-5, and 95-5 cruises are generally lower than for samples of similar thickness in the Arctic, despite high surface salinities and higher sea-water salinities, and contrary to what has been previously thought for antarctic ice (Doronin and Kheisin 1975). A possible explanation is that the relatively warm ice in this region allows for freer movement of the brine and, thus, more efficient desalination of the ice. Because the lower layers of the thicker ice were generally near the freezing point of sea water, the brine salinity would be quite close to that of the underlying sea water, and so gravity drainage would no longer be effective. This ice may then have reached its minimum salinity and so does not show any further decrease of bulk salinity with increasing core length. The thinner ice was generally young cold ice and consequently may have undergone less vigorous desalination than the thicker ice. Cruise 95-3 was early in the growth season, so many of the cores were taken from younger ice than the late winter cores. The younger ice formed under cold conditions and should show salinities more in line with those for arctic ice.

To examine temporal and spatial variations, cores were selected from two regions for which data had been collected from two separate cruises: the Ross Sea, and the Amundsen and Bellingshausen Seas, as indicated in figure 1. Figure 3A shows bulk salinity versus core length for the same region of the Ross Sea in early and late winter 1995. Despite the scatter, salinities are similar to those expected for arctic ice. The only clear difference between the two data sets is the significantly greater core lengths of the late winter data, as one would expect. Figure 3C shows data from late winter 1993 and 1995 in the Amundsen and Bellingshausen Seas. A clear trend is evident because these data exhibit significantly less scatter. Both years of data have very similar characteristics; it is postulated that ice growth and desalination conditions remain quite similar from year to year in this region. In contrast to the Ross Sea region, ice of moderate thickness (40 to 100 cm) clearly shows low salinities as compared to arctic values. Most of these samples were very warm and, as noted above, have probably undergone marked desalination.

Figures 3B and 3D show normalized probability density functions of bulk salinity and give a clearer picture of the salinity distribution. The two data sets for the Amundsen and Bellingshausen Seas show very similar characteristics and have a large narrow peak at a salinity of about 5 ppt. This peak is lower than in the Ross Sea, where salinity peaks at about 6 ppt in late winter, compared to the much broader peak at about 6.5 ppt in early winter. The broadness of the latter peak can be attributed to a large contribution from younger saline ice rapidly forming in cold conditions in the more northern regions of the Ross Sea. Older ice, either in

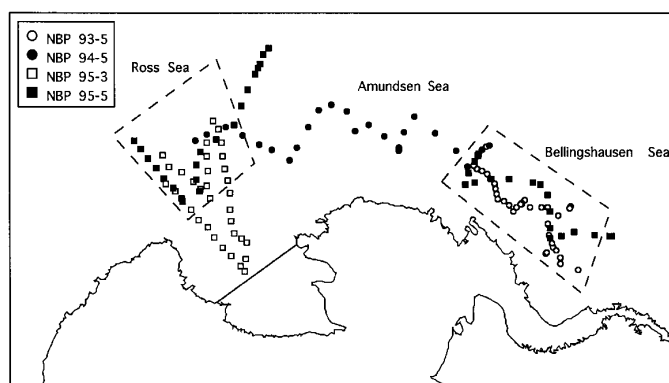


Figure 1. Map of the Pacific sector of the southern oceans showing ice floe sampling sites for each of the four cruises. Typically, 3–5 cores were obtained at each floe site. Cruise NBP95-3 was in May and June. The other cruises were in August, September, and October. The two boxed regions show the areas for which a regional comparison has been made.

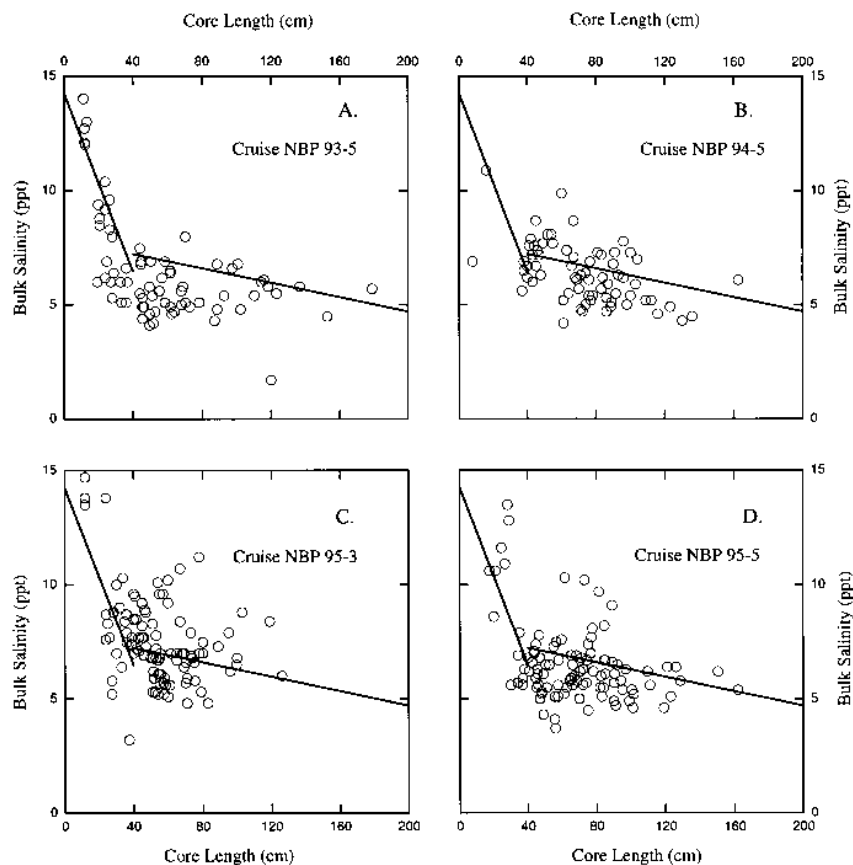


Figure 2. Bulk ice-core salinity values plotted against core length for each of the four cruises. The solid lines show regression fits for first-year arctic ice (Cox and Weeks 1974).

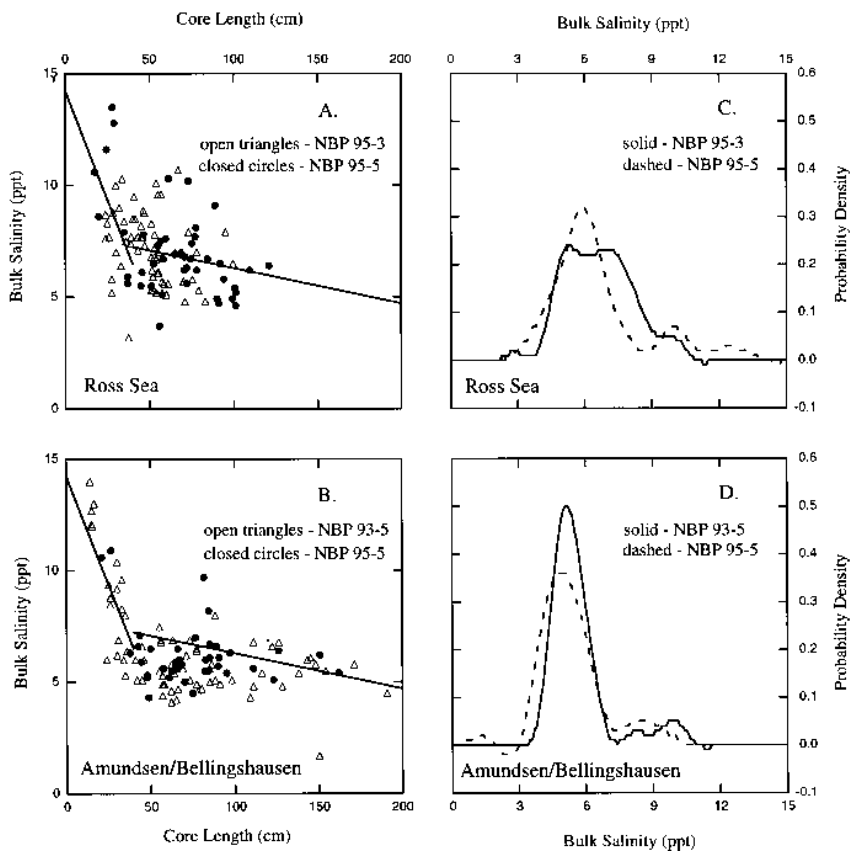


Figure 3. Comparison of bulk ice-core salinity values for the two selected regions shown in figure 1. (A) Bulk salinity versus core length for the northern Ross Sea for early and late winter 1995. (B) Bulk salinity versus core length for the Amundsen and Bellingshausen Seas for late winter 1993 and 1995. (C and D) The corresponding probability distribution functions of salinity values.

the southern sector or in late winter, show lower salinities with a narrower distribution.

These data suggest that despite high surface salinities that probably result from snow ice formation, first-year sea ice of moderate thickness in the Pacific sector of the southern oceans shows comparatively low bulk salinity due to efficient desalination.

This research was supported by National Science Foundation grants OPP 91-17721 and OPP 93-16767. We would like to thank the many individuals of the science

teams, Antarctic Support Associates, and Edison Chouest Offshore who contributed to the collection of the data.

References

- Cox, G.F.N., and W.F. Weeks. 1974. Salinity variations in sea ice. *Journal of Glaciology*, 13(67), 109–120.
- Doronin, Y.P., and D.E. Kheisin. 1975. *Sea ice*. Y.U. Kathavate and V.S. Kothekar (Translators, 1977). Faridabad, India: Oxonian Press.
- Eicken, H. 1992. Salinity profiles of antarctic sea ice: Field data and model results. *Journal of Geophysical Research*, 97(C10), 15545–15557.

Bottom water distribution in the Weddell Sea

ARNOLD L. GORDON, *Lamont-Doherty Earth Observatory, Palisades, New York 10964-8000*

As we collect more observational data, it is becoming increasingly evident that the ocean varies both spatially and temporally far more energetically than previously thought. Such is the case in the Weddell Sea, where detailed observations within its western rim from the Ice Station Weddell (ISW Group 1993) exposed the co-existence of two types of bottom water, one relatively fresh, the other more saline. Often these two types are observed within a single station, forming a highly stratified benthic layer (Gordon et al. 1993). Using the ISW data and other recent data in the Weddell Sea, a more detailed map of bottom potential temperature and salinity is constructed (figures 1 and 2).

Within the deeper central part of the Weddell Sea, the bottom potential temperature pattern (figure 1) reveals the presence of relatively warm bottom water, above -0.8°C . This broad feature forms as water warmer than -0.8°C shifts toward the deeper center of the basin upon encountering the outflow of very cold and dense Ice Shelf Water from the Weddell Sea Shelf, channeled within the Filchner Depression (Foldvik, Gammelsrod, and Torresen 1985, pp. 5–20). The warm bottom water approaching from the east at depths below the mouth of the Filchner Depression [between 600 to 650 meters (m); map 567 from the AWI bathymetry series 1996] is pushed toward the central basin, while the warmer bottom water of the upper slope, first undercut by the colder water, reappears along the upper slope to the west of the cold-water plume, which drops to deeper levels while advecting westward.

A major export cold shelf water appears to occur just west of General Belgrano Bank (72.5° to 73.5°S and 47° to 50°W). From that point, the areal extent of the seafloor deeper than 1,000 m covered with cold bottom water (below -1.0°C) grows progressively larger along the general flow path of the Weddell Gyre toward the west and north (Muench and Gordon 1995). Most of the ISW bottom temperatures in the western Weddell Sea at depths of 2,500 to 3,000 m, south of

67°S is well below -1.2°C . North of 67°S , the width of the colder than -1.4°C bottom layer abruptly narrows, an effect that may be a product of increased vertical mixing with slightly warmer overlying water (Gordon et al. 1993). In the north-western Weddell Sea, cold bottom water turns toward the east as water colder than -1.0°C near 64°S and continues eastward as water colder than -0.9°C between 64° and 66°S .

The bottom salinity distribution (figure 2) in the western Weddell Sea reveals the spatial distribution of the two types of bottom waters. A plume of less than 34.62 bottom water emanates from just west of General Belgrano Bank, winding itself along a path of 700 kilometers toward the north, ending near 65°S and 50°W . The saline shelf water of the western Weddell Sea (Western Shelf Water, Foldvik et al. 1985, pp. 5–20), migrates northward, escaping from the shelf near 69°S , forming a saline plume just landward of the less than 34.62 plume. The ISW stations (Gordon et al. 1993) show that this salty bottom water lifts the lower salinity bottom water off the seafloor, inducing a very stratified double-layer slope plume. It is suspected that slope canyon near 70°S directs the saline shelf water into the deep ocean.

Seaward of the elongated less than 34.62 plume, there is a suggestion of a plume of greater than 34.65 water. It is expected that the Filchner Depression outflow of Ice Shelf Water entrains some of the older more saline bottom water advected in from the east. This mixture is still colder than the -0.8°C water of the central Weddell Basin.

In summary, bottom water characteristics reveal major export of low-salinity shelf water near 72°S 51°W immediately west of General Belgrano Bank. It is joined downstream by high-salinity bottom water just north of 70°S . The low-salinity bottom water is expected to be derived from Ice Shelf Water, similar to the export from Filchner Depression; the high-salinity bottom water is derived from the mass of Western Shelf Water, a product of sea-ice formation. Only in the western Weddell Sea do these two types of bottom waters stratify

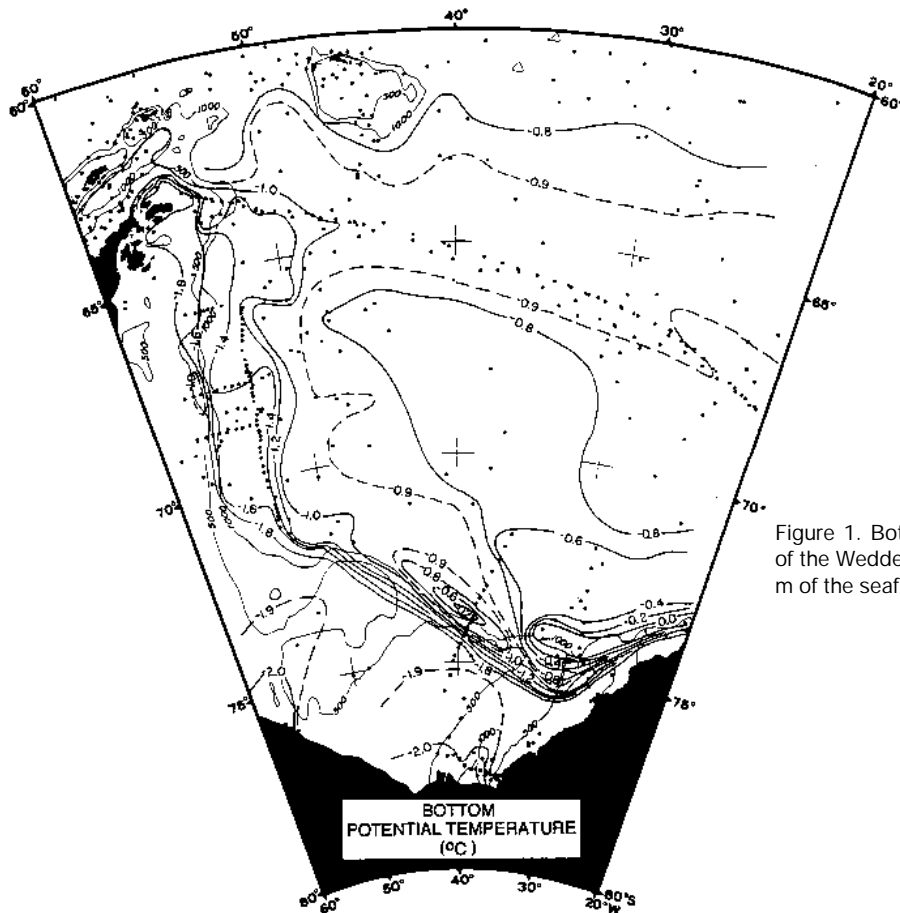


Figure 1. Bottom potential temperature of the Weddell Sea. Values are within 50 m of the seafloor.

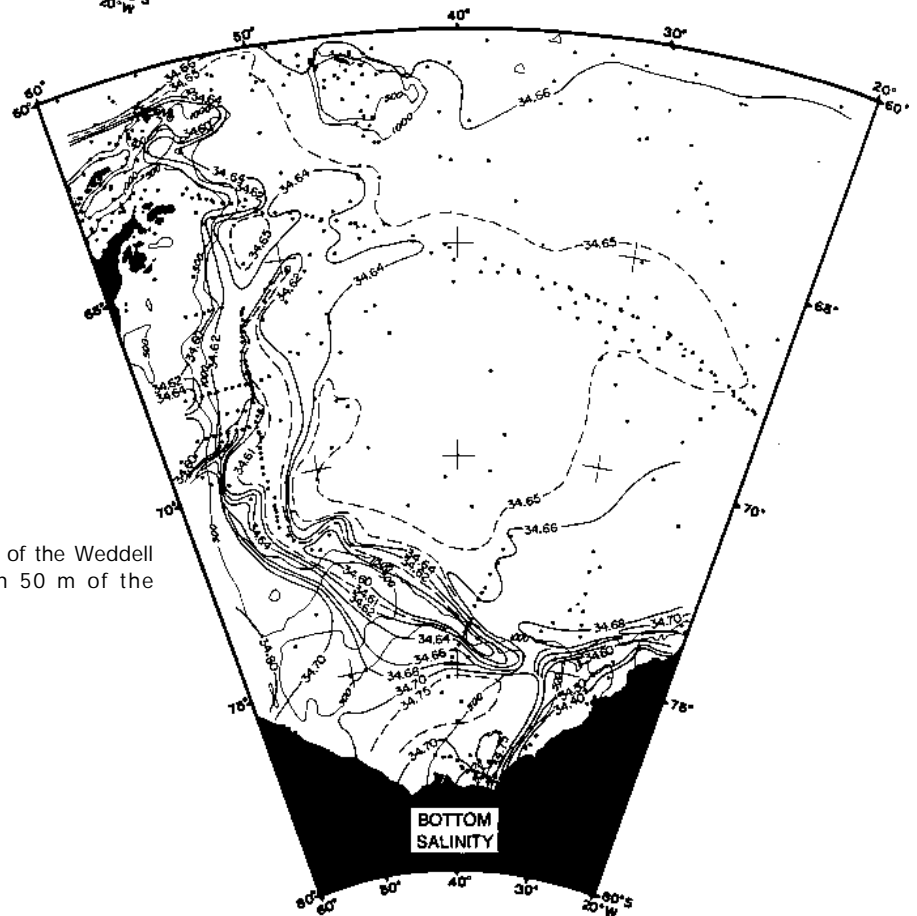


Figure 2. Bottom salinity of the Weddell Sea. Values are within 50 m of the seafloor.

to occupy the same water column. One wonders if the ratio of low- to high-salinity bottom water changes with time, perhaps in response to sea-ice changes.

The ISW research is supported by National Science Foundation grant OPP 93-13700.

References

- Alfred-Wegener-Institute for Polar and Marine Research. 1996. *AWI bathymetric charts of the Weddell Sea, Antarctica* (AWI BCWS map 567). Bremerhaven, Germany: Alfred-Wegener-Institute.
- Foldvik, A., T. Gammelsrod, and T. Torresen. 1985. Circulation and water masses on the southern Weddell Sea shelf. In S.S. Jacobs (Ed.), *Oceanology of the antarctic Continental Shelf* (Antarctic Research Series, Vol. 43). Washington, D.C.: American Geophysical Union.
- Gordon, A.L., B.A. Huber, H.H. Hellmer, and A. Field. 1993. Deep and bottom water of the Weddell Sea's western rim. *Science*, 262, 95-97.
- ISW Group. 1993. Weddell Sea exploration from ice station. *EOS, Transactions of the American Geophysical Union*, 74(11), 121 & 124-126.
- Muench, R.D., and A.L. Gordon. 1995. Circulation and Transport of Water Along the Western Weddell Sea Margin. *Journal of Geophysical Research*, 100, 18503-18515.

Profiling the South Pacific antarctic continental shelf

C. GIULIVI and S. JACOBS, *Lamont-Doherty Earth Observatory of Columbia University, Palisades, New York 10964*

Field support of a biogeochemical study in the Ross Sea polynya continued on *Nathaniel B. Palmer* cruise 9508, with 150 conductivity-temperature-depth (CTD) stations taken during December 1995 and January 1996 in the south-west Ross Sea (figure 1). Three long sections were reoccupied along 76.5°S, as were three short transects along 165°E and 172°E, and several casts were made directly north of Ross Island (approximately 77.5°S 168°E). Eighty-six of the stations reached within a few meters of the seafloor, thereby accessing

a bottom boundary layer that often displays higher turbidity and salinity (Jacobs 1989). Equipment and water-sampling procedures were as described in Jacobs et al. (1995), and the data from *Nathaniel B. Palmer* cruise 9406 appear in Giulivi et al. (1995). The sea surface was sampled for oxygen isotopes while the ship was enroute to the Ross Sea from Lyttleton, New Zealand.

Work also continued on other southern ocean data obtained on the *Palmer* and USCGC *Polar Sea*. Representative

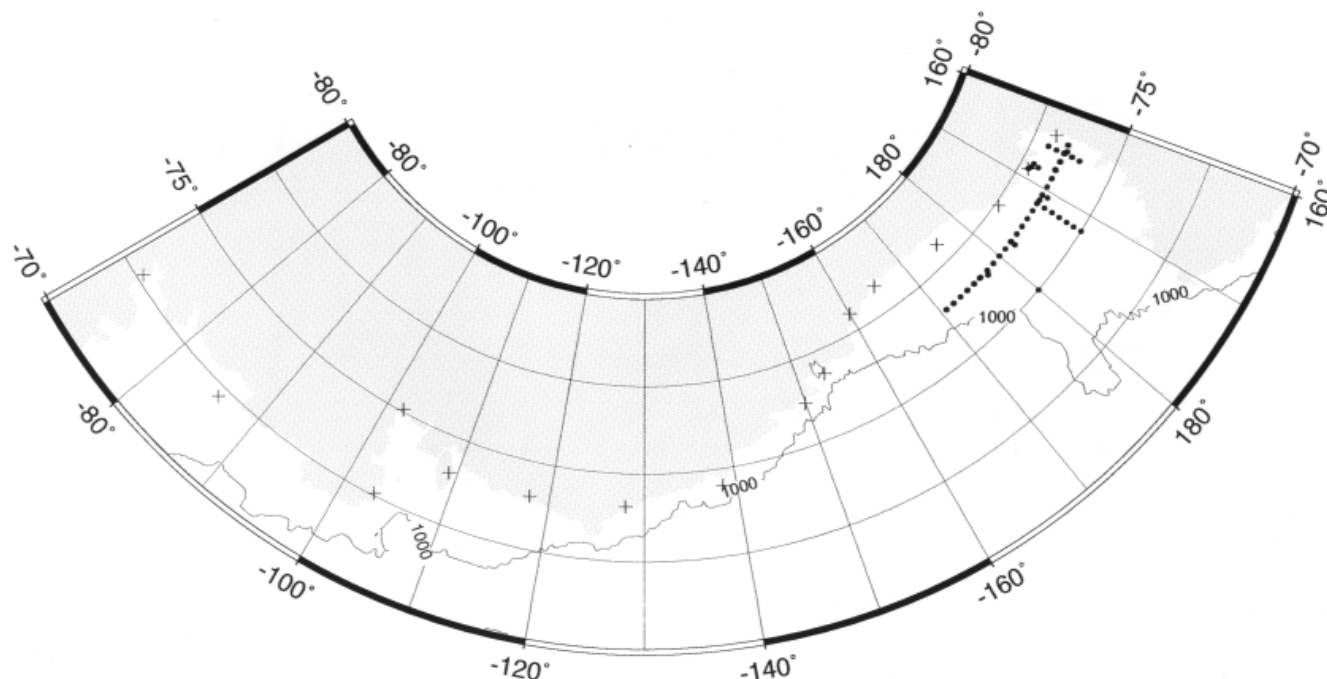


Figure 1. The locations of CTD stations occupied on *Nathaniel B. Palmer* cruise 9508 (dots) and selected stations from *Palmer* 9402 and *Polar Sea* 94 (crosses), near the southern limit of the Pacific Ocean. The edge of the antarctic ice sheet (shaded) and the 1,000-m bathymetric contour roughly define the limits of the open continental shelf from 70° to 80°S and 70°W to 160°E.

coastal stations from those cruises (figure 1) reveal a temperature field that varies substantially from the Antarctic Peninsula to the Ross Sea (figure 2). Relatively warm Circumpolar Deep Water and its derivatives flood the deeper parts of the continental shelf in the Bellingshausen and Amundsen Seas. Colder shelf water west of the central Amundsen Sea is caused by more rapid sea-ice removal and greater surface freezing in the Ross Sea polynya and in smaller but similar coastal features. Typically, perennial and snow-covered sea ice over the continental shelf in the Amundsen and Bellingshausen Seas is believed to result, in part, from more onshore winds in that sector. Sea-ice extents in this region reached record lows during the late 1980s and early 1990s (Jacobs and Comiso in press) but returned to the two-decade mean extent by the first half of 1996.

The warmer Circumpolar Deep Water at depth in the eastern region of figure 2 leads to much higher melt rates of the small floating ice shelves and many icebergs in that sector. The colder but lighter deep water/meltwater mixture upwells into the near-surface layers and may contribute to shoaling of the -1.5°C isotherm in the Amundsen Sea. Oceanic melting at the base of Pine Island Glacier, near station 92, averages more than 10 meters per year, roughly equivalent to its iceberg calving rate (Jacobs, Hellmer, and Jenkins 1996; Jenkins et al. in press). A numerical model of the sub-ice circulation suggests local melt rates in excess of 20 meters per year, and chemical analyses of the outflow indicate that precipitation on the glacier catchment basin will

have an oxygen-18 ratio of approximately -29‰ (Hellmer, Jacobs, and Jenkins in press).

The shipboard support on *Palmer* 9508 was carried out by J. Ardai and S. O'Hara. CTD data reduction and analysis is supported by National Science Foundation grant OPP 94-18151; sub-ice shelf modeling by Department of Energy grant DE FG02 93ER61716; sea-ice research by National Aeronautics and Space Administration grant NAGW 3362.

References

- Giulivi, C., S. Jacobs, S. O'Hara, and J. Ardai. 1995. *Ross Sea Polynya Project, 1994, Oceanographic Data, N.B. Palmer cruise 9406* (Technical report LDEO-95-1). Palisades, New York: Lamont-Doherty Earth Observatory.
- Hellmer, H., S. Jacobs, and A. Jenkins. In press. Ocean erosion of a fast-moving antarctic glacier in the Amundsen Sea. *Deep-Sea Research*.
- Jacobs, S. 1989. Marine controls on modern sedimentation on the antarctic continental shelf. *Marine Geology*, 85(2/4), 121-153.
- Jacobs, S., and J. Comiso. In press. Climate variability in the Amundsen and Bellingshausen Seas. *Journal of Climate*.
- Jacobs, S., C. Giulivi, S. O'Hara, and J. Ardai. 1995. Plumbing the Ross Sea polynya. *Antarctic Journal of the U.S.*, 30(5), 197-199.
- Jacobs, S., H. Hellmer, and A. Jenkins. 1996. Antarctic ice sheet melting in the Southeast Pacific. *Geophysical Research Letters*, 23(9), 957-960.
- Jenkins, A., D. Vaughan, S. Jacobs, H. Hellmer, and J. Keys. In press. Glaciological and oceanographic evidence of high melt rates beneath Pine Island Glacier, West Antarctica. *Journal of Glaciology*.

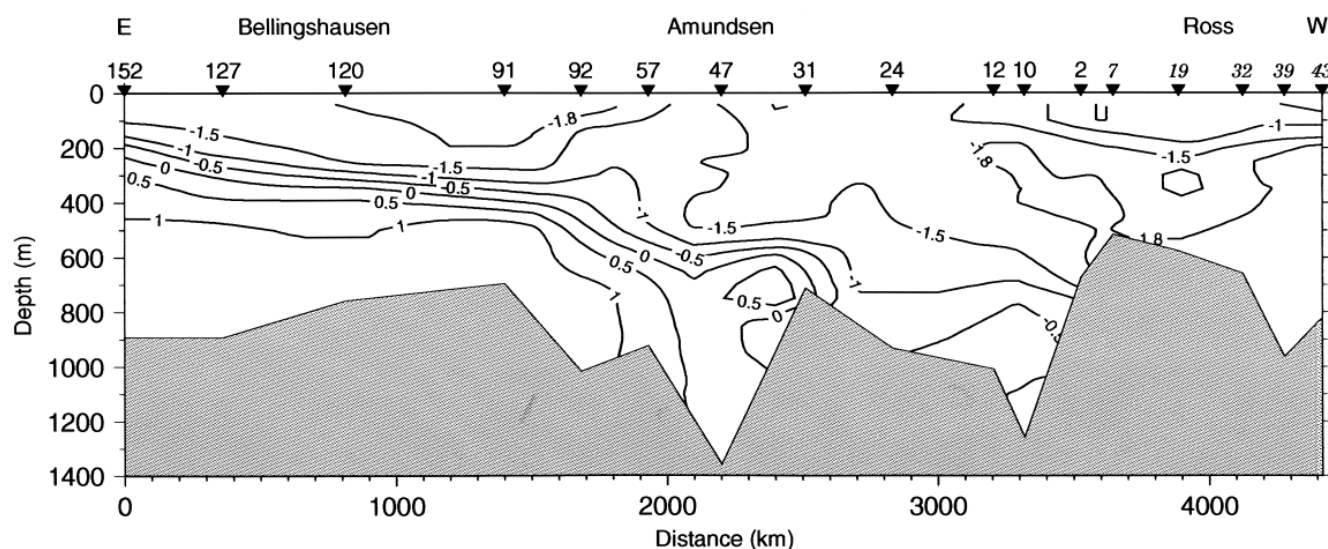


Figure 2. Temperature field near the antarctic coastline in February and March 1994, as defined by CTD stations at the crosses in figure 1. [The easternmost station (152) was in Marguerite Bay (approximately 68.5°S 68.5°W), off the upper left of figure 1.] Temperatures are in degrees Celsius; distances (in kilometers) are along great circles between CTD casts.

Light-saturated primary production in antarctic coastal waters

MARK A. MOLINE, *Institute of Marine and Coastal Sciences, Rutgers University, New Brunswick, New Jersey 08903-0231*

BARBARA B. PRÉZELIN, *Marine Primary Productivity Group, Department of Biological Sciences, University of California, Santa Barbara, California 93106*

HERVÉ CLAUSTRE, *Laboratoire de Physique et Chimie Marines, Villefranche-sur-mer, France*

During the austral spring and summer seasons from 1991 to 1994, 756 discrete water samples were collected at the Palmer Long-Term Ecological Research (LTER) program stations B and E (Moline and Prézelin 1997a). For each discrete sample, photosynthesis-irradiance (P-I) relationships ($n=25$) were determined. Photosynthetic parameters P_{\max} (the light saturated photosynthetic potential), α (the light-limited photosynthetic efficiency), I_k ($=P_{\max}/\alpha$; an estimate of the minimum irradiance required for the onset of light-saturated photosynthesis), β (the efficiency of photoinhibition), and I_t (the irradiance threshold for the onset of photoinhibition) were derived from the P-I relationships and then used to calculate primary production for each discrete sample. The diel patterns of each parameter were also measured weekly and incorporated into the production calculations to produce daily rates of primary production throughout the water column over the 3-year sampling period. Q_{par} [400–700 nanometers (nm)] irradiance values for the productivity calculations were obtained by integrating surface/in-water irradiance measurements taken while sampling and incident irradiance recorded continuously every 5 minutes at Palmer Station over the three sampling seasons. Primary production estimates were also calculated using theoretical clear-sky Q_{par} irradiance, calculated from Morel (1991) and Antoine (personal communication) using an atmospheric correction (350 dobson units for ozone content and 2 centimeters precipitable water content). Light-saturated primary production was quantified as the fraction of production operating at P_{\max} at an irradiance greater than the measured value of I_k . Further details of sample collection and analyses are described elsewhere (Claustre, Moline, and Prézelin in press; Moline and Prézelin 1997a,b).

Primary production for the nearshore LTER stations showed significant variability with each season and between years (figure 1A). Much of the seasonal variability was the result of fluctuations in biomass as a result of advective processes and vertical mixing within the water column (Moline and Prézelin 1997b). The temporal changes in the taxonomic structure of the water column also significantly affected the measured rates of carbon uptake (Claustre et al. in press). High interannual variability resulted from differences in the stability and durations of low wind speeds between years. Significantly higher production was measured during a large diatom bloom in December 1991 (figure 1A). The percentage of primary production that was light-saturated over the three spring and summer periods averaged 47 ± 17 (figure 1B). A seasonal trend was evident; peak saturation occurred during the peak solar irradiance and a generally

lower percentage of saturation occurred earlier and later in the year. During the 1991–1992 bloom, light-saturated production was lower and may have been a result of light limitation by self-shading (Moline et al. 1997, pp. 67–72; Moline and Prézelin 1997a).

Cloud cover significantly decreased the incident surface irradiance by an average of 37 ± 24 percent from clear sky conditions and was consistent between years (figure 2A). On occasions, measured irradiance was higher than modeled clear-sky irradiance, probably resulting from light reflectance off surrounding snow cover and glaciers in this coastal envi-

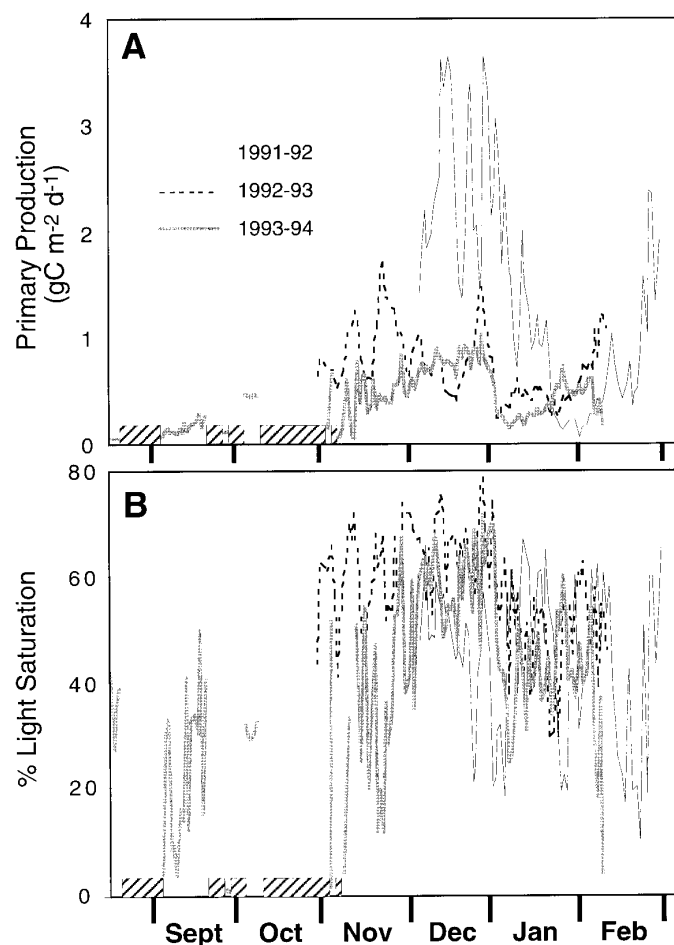


Figure 1. (A) Average daily depth-integrated primary production measured at stations B and E and (B) the percent of light-saturated primary production for three austral springs and summers between 1991 and 1994. Hatched bars indicate the presence of sea ice during the 1993–1994 season. ($\text{gC m}^{-2} \text{d}^{-1}$ denotes grams of carbon per square meter per day.)

ronment. The decrease in surface irradiance from cloud cover was estimated to decrease water column primary production by as much as 73 percent (November 1994) with an average of 20 ± 17 percent for all three seasons (figure 2B).

Light-saturated primary production was also calculated using modeled clear-sky irradiance. When the effect of cloud cover was removed, the percent light saturation increased by 8.4 ± 9.8 percent (figure 2C). No seasonal trends were evident; however, the percentage of change in the light-saturated primary production during the 1991–1992 season was not as great as the following two seasons. This smaller change may have been a result of the high *in situ* light attenuation due to high biomass during the bloom (December 1991 to January 1992) and toward the end of the sampling season in February 1992 (figure 1A).

The relatively small increase in the light-saturated production compared to the increase in irradiance when cloud

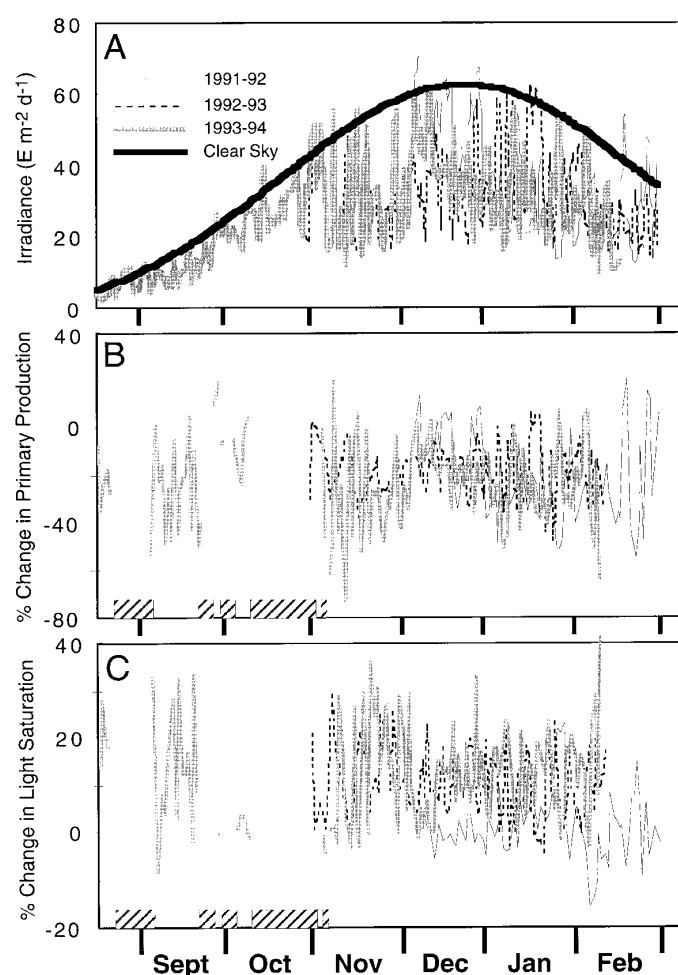


Figure 2. (A) Daily surface Q_{par} irradiance measured at Palmer Station during the austral springs and summers of 1991–1994. Also included is the modeled daily surface Q_{par} irradiance calculated for clear-sky conditions (thick solid line). (B) The percentage of change in primary production resulting from the presence of cloud cover over the 3 years. (C) The percentage of change in light-saturated production when the effect of cloud cover on surface irradiance is removed. Hatched bars indicate the presence of sea ice during the 1993–1994 season. ($\text{E m}^{-2} \text{ d}^{-1}$ denotes einsteins per square meter per day.)

cover was removed shows that the majority of production in these coastal waters was light-saturated over the season and also that light saturation was at a maximum. This finding is further illustrated by comparing the percentage of light saturation (calculated using the measured irradiance values) to the measured daily irradiance for all sampling days over the 3-year period (figure 3). For samples collected in open water, the maximum percentage of light-saturated production increased with increasing light. The percent saturation itself, however, saturated (at approximately 70–75 percent) at irradiances greater than 20–25 einsteins per square meter per second ($\text{E m}^{-2} \text{ s}^{-1}$). These irradiance levels indicate that these phytoplankton have the potential of being light-saturated from the end of September to the middle of March, nearly the full growing season in these polar waters. This long growing season may result from both the value of I_k (and depth within the water column where the irradiance is equal to I_k) and the fact that for a portion of the day, light is not saturating. Therefore, approximately 25–30 percent of water column primary production occurs below the depth where $I_k = Q_{\text{par}}$ and/or in the early and late hours of the daily solar cycle. Samples taken when the region was ice covered did not begin to show light saturation until daily irradiance values were above approximately $50 \text{ E m}^{-2} \text{ s}^{-1}$.

Results from this highly resolved temporal study quantify light-saturated primary production in this coastal region and show that these phytoplankton are generally light-saturated during most of the growing season from September to March. These results also argue against light-limitation being a major factor limiting primary production in the southern oceans.

Special thanks go to S. Roll, K. Seydel, and K. Scheppe for assistance in the field. H.A. Matlick provided technical assistance. This work was supported by National Science Foundation grant OPP 90-11927 awarded to Barbara B. Prézelin. This is Palmer LTER contribution 110.

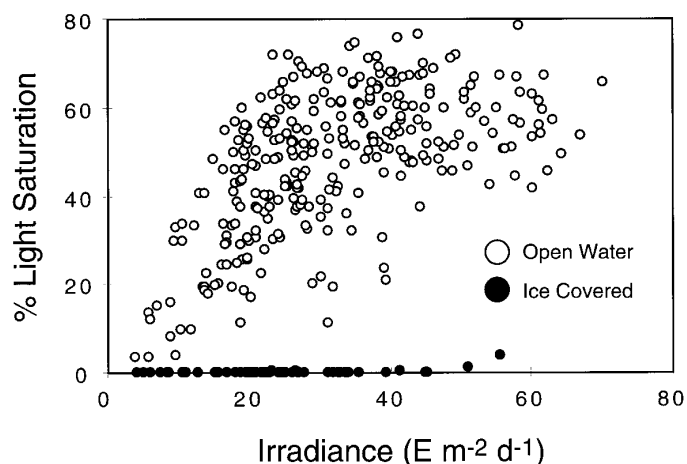


Figure 3. The percentage of light-saturation as a function of daily surface Q_{par} irradiance for all sampling days during the austral springs and summers of 1991–1994. ($\text{E m}^{-2} \text{ d}^{-1}$ denotes einsteins per square meter per day.)

References

- Antoine, D. 1996. Personal communication.
- Claustre, H., M.A. Moline, and B.B. Prézélin. In press. Sources of variability in the column photosynthetic cross section for antarctic coastal waters. *Journal of Geophysical Research*.
- Moline, M.A., and B.B. Prézélin. 1997a. High-resolution time-series data for 1991/1992 primary production and related parameters at a Palmer LTER coastal site: implications for modeling carbon fixation in the southern ocean. *Polar Biology*, 17, 39–53.
- Moline, M.A., and B.B. Prézélin. 1997b. Palmer LTER 1991–1994: Long-term monitoring and analyses of physical factors regulating variability in coastal antarctic phytoplankton biomass, *in situ* productivity and taxonomic composition over subseasonal, seasonal and interannual time scales. *Marine Ecology Progress Series*, 145, 143–160.
- Moline, M.A., B.B. Prézélin, O. Schofield, and R.C. Smith. 1997. Temporal dynamics of coastal antarctic phytoplankton: Environmental driving forces through a 1991–1992 summer diatom bloom on the nutrient and light regime. In B. Battaglia, J. Valencia, and D.W.H. Walton (Eds.), *Antarctic communities*. Cambridge: Cambridge Press.
- Morel, A. 1991. Light and marine photosynthesis: A spectral model with geochemical and climatological implications. *Progress in Oceanography*, 26, 263–306.

Radium-226/barium ratios for dating biogenic carbonates in the southern oceans: Preliminary evidence from coastal mollusk shells

PAUL ARTHUR BERKMAN, *Byrd Polar Research Center, Ohio State University, Columbus, Ohio 43210-1002*

TEH-LUNG KU, *Department of Geological Sciences, University of Southern California, Los Angeles, California 90089-0740*

The purpose of this preliminary study was to assess the viability of radium-226/barium ($^{226}\text{Ra}/\text{Ba}$) as an alternative to carbon-14/carbon-12 ($^{14}\text{C}/^{12}\text{C}$) for dating marine fossils that have circumpolar distributions in raised beaches and reflect environmental events around Antarctica during the Holocene (Berkman 1992). The similarity in the water column marine geochemistry between ^{226}Ra and Ba is such that barium can be treated as a stable “isotope” of ^{226}Ra for dating materials in the same manner as $^{14}\text{C}/^{12}\text{C}$ ratios (Broecker and Peng 1982). The stimulus for this study was the uncertainty, which may be hundreds of years, in correcting the radiocarbon reservoir for dating biogenic materials in the southern oceans (Berkman and Forman 1996).

Radium-226 (half-life, 1,620 years) enters the ocean mostly via diffusion across the sediment-water interface where a large concentration gradient of ^{226}Ra exists because of the deposition of its radioactive precursor, the particle-borne ^{230}Th (Ku and Luo 1994). Because of the relatively intense vertical mixing in the circumantarctic region, surface-water ^{226}Ra concentrations are within 30 percent of the deep-water values (Ku et al. 1970; Ku and Lin 1976). This contrasts with situations in the low-latitude oligotrophic oceans, where the surface and deep concentrations may differ by a factor as large as six. Radium/calcium (Ra/Ca) ratios for marine mollusk shells can vary directly with sea-water Ra/Ca ratios but are strongly influenced by the species and their carbonate mineralogy (Blanchard and Oakes 1965). Around Antarctica, the scallop (*Adamussium colbecki*) is among the most common coastal marine mollusks having extant assemblages that can serve as experimental analogs for interpreting the geochemistry of adjacent fossils in raised beaches.

Calcitic shells of living *Adamussium* have unit-cell dimensions that are larger than those in pure calcite crystals (Berkman et al. 1992). These unit-cell data reflect isomorphic substitutions in the carbonate matrix by divalent cations that have larger ionic radii than calcium: namely, barium, strontium, or radium. Primarily for this reason, preliminary $^{226}\text{Ra}/\text{Ba}$ analyses were conducted with *Adamussium* shells that were collected alive using scuba gear in Explorers Cove (77°35'S 163°40'E), Antarctica, during the 1986–1987 austral summer.

Similar size *Adamussium* shells (79.7±4.8 millimeters in height) were analyzed for ^{226}Ra to eliminate any geochemical variations that may be associated with their ontogeny. Because the *Adamussium* shells are wafer thin [3–4 grams (g) each], several shells were combined to obtain the 25–35-g batches of carbonate for the ^{226}Ra measurements by alpha-scintillation counting with the Rn-emanation method at the University of Southern California (Ku et al. 1970). The shells were either cleaned with distilled water or dilute acid before being roasted at 500°C. Complementary analyses of calcium and barium were conducted by inductively coupled plasma spectrometry at the University of Michigan on 12 acid-cleaned shells from Berkman (1994, pp. 11–33). The results are listed in the table.

The concentration of ^{226}Ra can be predicted in the *Adamussium* shells in relation to calcium, which has a sea-water concentration of approximately 400 milligrams per kilogram (mg kg⁻¹). The ^{226}Ra concentration in antarctic surface (0–100 meters) sea water is 0.18 disintegrations per minute per kilogram (dpm kg⁻¹; GEOSECS station 287 at 69°18'S 173°30'W; Ostlund et al. 1987). If ^{226}Ra and Ca were incorporated from sea water into the *Adamussium* shells without fractionation, then 1 g of shell (400 mg calcium + 120 mg car-

Radium, calcium, and barium concentrations in modern antarctic scallop (*Adamussium colbecki*) shells

Adamussium preparation	Sample weight	Analytical method	²²⁶ Ra (dpm g ⁻¹)	Ca (mg g ⁻¹)	Ba (μg g ⁻¹)
Acid cleaning	32.1 g	Rn-emanation (two trials)	0.035±0.002 0.040±0.002	—	—
Acid cleaning	25.7 g	Rn-emanation (fraction 2a)	0.039±0.002	—	—
No-acid cleaning	24.3 g	Rn-emanation (fraction 2b)	0.041±0.002	—	—
Acid cleaning	N=12 ^a	Inductively coupled plasma	—	396.92±0.47	2.28±0.40

^aLess than 100-mg aliquots of shell powder from each of the 12 individual *Adamussium* shells from Berkman (1994) were analyzed.

bon + 480 mg oxygen) would have 0.18 dpm. Based on the data in the table, the ²²⁶Ra concentrations in the *Adamussium* shells ranged narrowly from 0.035 to 0.041 dpm g⁻¹, which points to an apparent discrimination factor of 4.4 to 5.1 against ²²⁶Ra relative to Ca in the shell formation.

The concentration of barium in antarctic surface sea water at GEOSECS station 287 is approximately 10.7 micrograms per kilogram (μg kg⁻¹) (Ostlund et al. 1987). The measured concentration of Ba in the dilute acid-cleaned batch of *Adamussium* shells was 2.28±0.40 μg g⁻¹, a level that indicates that Ba was being discriminated against by a factor of 4.7±0.8, a result similar to that of Ra-Ca.

These preliminary analyses indicate that the ²²⁶Ra/Ba ratios in the sea water and shells were maintained, even though the absolute concentrations of the elements were discriminated against by a factor of roughly 4.5 to 5.0 relative to Ca during the shell formation. Moreover, the consistent discrimination between acid-treated and mechanically treated shells along with the small variability within batches of mixed shells supports the suggestion that ²²⁶Ra and Ba are being incorporated into the intracrystalline lattice sites of the unit cells in *Adamussium* shell calcite. Together, these data suggest that *Adamussium* shells may be treated as a closed system for ²²⁶Ra and Ba with an initial ²²⁶Ra/Ba ratio close to that of the ambient sea water.

This study indicates that it may be viable to develop a ²²⁶Ra/Ba chronometer for dating calcareous marine fossils in the southern oceans up to several thousand years of age. More precise analyses are being conducted in collaboration

with scientists from Lamont-Doherty Earth Observatory (W.S. Broecker, G. Henderson, and S. Peacock) and Open University in England (A.S. Cohen) who are analyzing the ²²⁶Ra and Ba in individual *Adamussium* shells by thermal ionization mass spectrometry (Cohen and O'Nions 1991).

This study was supported by a grant from the National Science Foundation (OPP 92-21784) to P.A. Berkman. We also would like to thank Yuhong Tang for his assistance with the ²²⁶Ra analyses.

References

- Berkman, P.A. 1992. Circumpolar distribution of Holocene marine fossils in antarctic beaches. *Quaternary Research*, 37, 256–260.
- Berkman, P.A. 1994. *Geochemical signatures of meltwater in mollusc shells from antarctic coastal areas during the Holocene* (Memoirs of the National Institute of Polar Research, Special issue no. 50.) Tokyo: National Institute of Polar Research.
- Berkman, P.A., and Forman, S.L. 1996. Pre-bomb radiocarbon and the reservoir correction for calcareous marine species in the southern ocean. *Geophysical Research Letters*, 23, 363–366.
- Berkman, P.A., D.W. Foreman, J.C. Mitchell, and R.J. Liptak. 1992. Scallop shell mineralogy and crystallographic characteristics: Proxy records for interpreting antarctic nearshore marine hydrochemical variability. In David Elliot (Ed.), *Contributions to antarctic research III* (Antarctic Research Series, Vol. 57.) Washington, D.C.: American Geophysical Union.
- Blanchard, R.L., and D. Oakes. 1965. Relationships between uranium and radium in coastal marine shells and their environment. *Journal of Geophysical Research*, 70, 2911–2921.
- Broecker, W.S., and T.-H. Peng. 1982. *Tracers in the sea*. Palisades, New York: Eldigio Press.
- Cohen, A.S., and R.K. O'Nions. 1991. Precise determination of femto-gram quantities of radium by thermal ionization mass spectrometry. *Analytical Chemistry*, 63, 2705–2708.
- Ku, T.-L., Y.H. Li, G.G. Mathieu, and H.K. Wong. 1970. Radium in the Indian-Antarctic Ocean south of Australia. *Journal of Geophysical Research*, 75, 5286–5292.
- Ku, T.-L., and M.C. Lin. 1976. Radium-226 distribution in the Antarctic Ocean. *Earth and Planetary Science Letters*, 32, 236–248.
- Ku, T.-L., and S. Luo. 1994. New appraisal of radium-226 as a large-scale oceanic mixing tracer. *Journal of Geophysical Research*, 99, 10255–10273.
- Ostlund, H.G., H. Craig, W.S. Broecker, and D. Spencer. 1987. *GEOSECS Atlantic, Pacific, and Indian Ocean expeditions: Shorebased data and graphics* (Vol. 7). Washington, D.C.: National Science Foundation.